Coastal Engineering 207 (2026) 104989

Contents lists available at ScienceDirect

Coastal Engineering

journal homepage: www.elsevier.com/locate/coastaleng

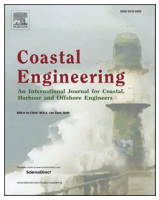

Optimizing long-term morphodynamic predictions in response to dominant forcing: A case study on the Belgian Continental Shelf

Yağız Arda Çiçek [a,*], Jaak Monbaliu [a], Erik Toorman [a], Víctor Cartelle [c], Ruth Plets [c], Nathalie Pil [d], Soetkin Vervust [d], Christian Schwarz [a,b]

[a] KU Leuven, Department of Civil Engineering, Kasteelpark Arenberg 40, 3001, Leuven, Belgium
[b] KU Leuven, Department of Earth and Environmental Sciences, Celestijnenlaan 200E, 3001, Leuven, Belgium
[c] Flanders Marine Institute (VLIZ), Jacobsenstraat 1, 8400, Oostende, Belgium
[d] Vrije Universiteit Brussel, Archaeology, Environmental Changes, and Geo-Chemistry (AMGC), Pleinlaan 2, 1050, Brussels, Belgium

ARTICLE INFO

Keywords:
Long-term morphological modelling
Coastal morphodynamics
MORFAC
TELEMAC

ABSTRACT

Accurate prediction of long-term morphodynamic evolution in mixed-energy coastal systems requires models that resolve key hydrodynamic processes and reproduce the correct sequence and magnitude of forcing events. However, determining what constitutes the 'correct' events remains challenging because the governing processes operate across a wide range of temporal scales. In this study, we develop a hydro-morphodynamic modelling framework based on the TELEMAC suite to simulate multi-decadal morphological changes along the Belgian Part of the North Sea (BPNS). After validation against hydrodynamic and suspended particulate matter observations, a 10-year benchmark run is used to establish a target morphology against which 43 tests to optimize boundary conditions for morphological acceleration using the MORFAC approach are evaluated. The optimization results show that predictive morphodynamic skill is linked to the co-occurrence of energetic wave events with the spring-neap tidal cycle. We subsequently introduce a new metric, the γ-factor, which quantifies the wave-tide interaction and can be used for MORFAC-based optimization. Optimal performance is achieved when synthetic wave series preserve the natural alignment of high-energy waves with spring tides, consistent with the benchmark run. In addition to the wave-tide timing (γ-factor), the optimization test shows that the predictive skill also depends strongly on the combined choice of *MORFAC* value and wave schematization. When applied to hindcast the 1984-2022 BPNS evolution, the optimized model reproduces the large-scale development of the deeper sandbanks but fails to capture the coastward migration of a shallower bank. This mismatch is attributed to missing wave-induced cross-shore sediment transport processes and is subsequently resolved by including effects of wave nonlinearity and Stokes-drift on sediment transport in the model equations. A final sensitivity analysis demonstrates a significant risk of model equifinality: an inaccurate representation of wave conditions and their temporal alignment with tidal cycles can still appear to produce correct morphological behaviour when compensated by parameter tuning, thereby hiding the shortcomings in the physical forcing. This underscores the need for physically informed and deliberate modelling choices when predicting long-term morphological changes.

1. Introduction

Coastal areas are highly dynamic environments where human activities and unique natural ecosystems co-exist (Zhang et al., 2012; Kroon et al., 2025; Neumann et al., 2015; Zhao et al., 2024). Managing trade-offs between coastal protection, economic development, recreational use and biodiversity requires a clear understanding of coastal morphological evolution (Barbier et al., 2011; Hoagland et al., 2023). This evolution is shaped by the interaction between natural forces occurring at multiple temporal and spatial scales (such as tides, surges, and waves) and human interventions (Roelvink et al., 2009; Wright and Thom, 2023). Because these natural and human drivers act simultaneously, it is challenging to distinguish cause and effect when assessing morphological changes. In this context, numerical models serve as valuable tools. They can predict the consequences of different management strategies or environmental change and can facilitate a deeper

* Corresponding author.
E-mail address: yagizarda.cicek@kuleuven.be (Y.A. Çiçek).

https://doi.org/10.1016/j.coastaleng.2026.104989
Received 12 December 2025; Received in revised form 20 February 2026; Accepted 23 February 2026
Available online 23 February 2026

understanding of drivers for short- and long-term morphodynamic development (De Vriend et al., 1993a, 1993b; He et al., 2022; Roelvink et al., 2001; Wang et al., 2014). Advances in computational power have facilitated the widespread use of complex numerical models (such as TELEMAC-GAIA (Tassi et al., 2023), Delft3D (Lesser et al., 2004), and XBeach (Roelvink et al., 2009)) to simulate 2-D and 3-D hydrodynamics and sediment transport in coastal systems (Dastgheib et al., 2008; Guillaume Olivier et al., 2021; Yin et al., 2019; Zhang et al., 2010). These numerical models, of which TELEMAC is used in this study, rely on solving systems of partial differential equations (PDEs), which impose numerical constraints on the choice of computational time steps, resulting in high computational demands. This is particularly problematic for long-term morphological predictions over decadal to centennial timescales (Kroon et al., 2025; Ranasinghe et al., 2011; Shaeri et al., 2019; Wang et al., 2014). While more efficient PDE solvers, GPU acceleration and local time stepping could mitigate these computational costs (Hu et al., 2025; Lyu et al., 2024; Zhao et al., 2025), establishing boundary conditions for periods lacking observational data persists as a critical challenge in long-term morphological modeling.

To reduce the high computational demand along with uncertainties in the boundary conditions for these predictions, several morphological acceleration methods have been developed (Roelvink, 2006). These techniques are usually based on the assumption that the morphological response of the system is much slower than its hydrodynamic response. Here, we focus on the most common techniques, i.e. tide-averaging, MorMerge and the MORFAC approach (Roelvink, 2006). The tide-averaging method freezes the morphology during computation and updates the bed-level after a tidal cycle using tide-averaged sediment transport quantities. The MorMerge method, on the other hand, uses a limited set of representative tide and wave conditions, created from statistics of measured data. Subsequently, these different forcings are applied to the same initial morphological configuration and predicted in parallel for a given time-step. At the end of the corresponding time-step the bed level change produced by the different forcings is merged into a combined morphology by weighting the bed level change per forcing with their occurrence. The new updated morphology is then used for the next time step for all the parallel runs (Boechat Albernaz et al., 2023). A third widely used technique for the morphological upscaling is the online morphological factor (*MORFAC*) approach (Lesser et al., 2004; Roelvink, 2006). It assumes that, within limits, morphological change caused by hydrodynamic forcing can be linearly upscaled in time. More specifically, for instance a morphological change predicted after 1s of hydrodynamics can be upscaled (e.g. using a *MORFAC* of 10) into 10s of morphological change by simply multiplying the bed level changes (Ranasinghe et al., 2011) or net sediment fluxes with the *MORFAC* (Mathew and Winterwerp, 2022). Hypothetically, the choice of the *MORFAC* magnitude is determined by the requirement that the morphological change created after updating the morphology (using the MORFAC method) should not significantly alter the flow pattern (Roelvink, 2006). In practice, the critical *MORFAC* is mostly determined experimentally, although there have been also attempts to determine it a priori (Ranasinghe et al., 2011).

An additional challenge in long-term morphological predictions is the choice of representative forcing conditions throughout the prediction period. Especially in the context of the discussed morphological upscaling techniques, considerations of the relevant dominant forcing factors (i.e. tides, surges, and waves) for a specific site need to be made. For instance, tide dominated systems were previously expressed using representative tide concept which focuses on finding one or more observed or synthetic tides that could reproduce the residual sediment fluxes caused by the difference between ebb and flood currents in real site conditions (Latteux, 1995; Schrijvershof et al., 2023). However, storm surges and wave conditions are more stochastic in time and therefore more difficult to schematize. Moreover, storm surge return intervals and magnitudes are often disregarded in long-term morphological simulations. This is in contrast with the various techniques that are available to represent wave conditions in long-term morphological simulations, such as finding a representative period reproducing averaged annual longshore sediment transport quantities (Kolokythas et al., 2023) or the use of wave energy flux method expressing the wave record based on the observed probability distribution (Roelvink et al., 2018). However, both methods compress long-term data into a limited set of conditions raising the question on how well such compressed datasets are able to capture morphological path dependency or the occurrence of extreme events that could lead to substantial morphological changes.

The present study focuses on the Belgian Part of the North Sea (BPNS), situated in the Southern Bight of the North Sea (Fig. 1), and characterized by an extensive system of tidal sandbanks (Deleu et al., 2004). This study is part of the TESTEREP Project, which investigates the Belgian Coastal evolution over the past 5 000 years through numerical modelling informed by geological and archaeological reconstructions. However, morphological modelling of such long time scales remains challenging due to the high computational demands and the uncertainties associated with the accurate representation of boundary conditions. In this context, several modelling studies have explored long-term morphological evolution along the BPNS. Around the Port of Blankenberge, both the Delft3D (Lesser et al., 2004) and XBeach (Roelvink et al., 2009) models achieved good agreement with a year-long observed morphological evolution, using a constant *MORFAC* combined with representative tide and synthetic wave forcing (Zimmermann et al., 2012). A similar study using Delft3D, on the other hand, applied the MorMerge approach for a 10-year simulation between Nieuwpoort and the Western Scheldt, and was able to reproduce general trends but failed to capture sandbank migration correctly (Wang et al., 2014). In a third study, a more comprehensive, two-non-cohesive sediment-class model was applied for the entire Belgian coast, using the TELEMAC modelling suite with representative tidal and wave forcing. It showed good agreement with the observed 10-year long morphological evolution near Zeebrugge (Kolokythas et al., 2023). Collectively, these studies highlight both the usefulness and limitations of morphological upscaling approaches, particularly regarding boundary data availability and sediment transport representation. However, they also demonstrate the absence of a consensus on the most suitable acceleration technique or representative forcings for the BPNS.

While the MORFAC method is widely used in morphodynamic models, its efficiency remains unclear in systems governed by regular (tides) and intermittent (waves, storms) forcing linked with non-linear wave-tide-surge interactions. Despite the complexity of mixed wave-tide energy systems, the specific impact of wave-tide timing, as well as the dominant sediment transport processes on long-term morphological evolution remain largely unexplored in the existing literature. In this study, we aim to address these gaps under three main sections summarized in Fig. 2. First (Section 2.2), we calibrated and validated a hydrodynamic and sediment transport model, the Belgian Coast Model (BCM), against field measurements from 2013. Following this section, the validated model was run for 11 years (2012 for spin-up and 2013-2023) using real flow and wave boundary conditions generated by a larger-scale hydrodynamic model (see Section 2.3). The resulting morphological changes were then used as a benchmark to systematically optimize the *MORFAC* value and the tide, surge, and wave boundary conditions of the accelerated model. Here, a new method is established to quantify the temporal alignment between field-observed wave conditions and spring-neap cycles. This methodology enables a more accurate representation of the hydrodynamic chronology within accelerated simulations forced by synthetic wave time series and spring-neap tides. The Brier Skill Score (*BSS*) and the percentage of matching erosion and deposition areas ($A_{m,\%}$) were used to evaluate the performance of the accelerated model against the benchmark simulation. Finally (Section 3.2), the optimized accelerated model was applied to hindcast the morphological evolution of the western Belgian Coast over the 1984-2022 period, allowing the identification of the dominant physical processes driving long-term coastal change and introducing

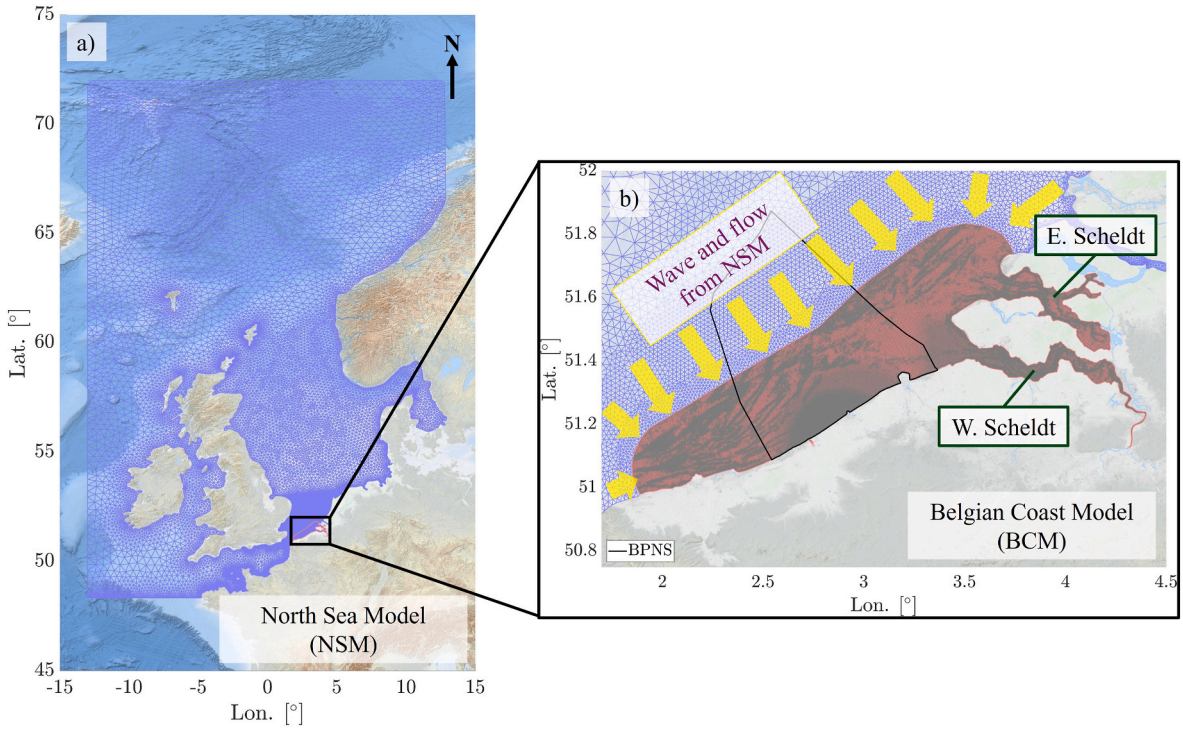

Fig. 1. (a) North Sea Model (NSM) domain (blue), (b) Belgian Coast Model (BCM) domain mesh elements (red and gray) and nesting procedure indicated with yellow arrows. The model domain covers parts of the French, BPNS (black solid line), and Dutch Coasts. Coordinate system is WGS84.

briefly the equifinality issue of the morphological models.

2. Materials and methods

2.1. Site characteristics

The Belgian coastline is approximately 65 km long, with a sandy nearshore seabed, beaches, and dunes. The BPNS is characterized by tidal and shoreface connected sand banks. These include the Coastal Banks (Nieuwpoortbank, Stroombank, Balandbank, Wenduinebank), Flemish Banks (Oostdyck, Buitenratel, Kwintebank, Middelkerkebank, Oostendebank), Hinder Banks (Fairy Bank, Westhinder, Noordhinder, Oosthinder, Bligh Bank) and the Zeeland Ridges (Thorntonbank, Gootebank, Akkaertbank) (Lanckneus et al., 2001) (Fig. 3). These sand banks are oriented shore-obliquely in the offshore (e.g. Kwintebank and Buitenratel) whereas closer to the coast their orientation becomes nearly shore-parallel (e.g. Nieuwpoortbank and Stroombank). Most of these banks display a general northeastward (longshore) migration, although Coastal Banks exhibit also cross-shore migration towards the coast (Dujardin et al., 2023). This study focuses on the zone hosting the Coastal Banks, which is characterized by complex hydrodynamics and sediment transport influenced by the local erosion of Palaeogene clay, causing the presence of clayey and coarse sandy sediments up to a median grain size of 500 μm (Lanckneus et al., 2001). The Coastal Banks have a landwards-directed steep slope (De Maeyer and Wartel, 1988; Van Lancker, 1999). The complex hydrodynamics in this zone are driven by tides, waves and storms combined with intense human activity, such as dredging, dumping and nourishments (Van Lancker et al., 2007), which prevent a clear understanding of the processes driving the sediment transport (Fig. SI–1). Therefore, morphodynamic modelling in this zone, especially over timescales from decades to centuries is a challenge for state-of-the-art models.

Tides in the BPNS are dominated by the M2, S2 tidal constituents forming the spring-neap variation with a mean spring and neap tidal range of 4.3 m and 2.8 m, respectively (Fettweis et al., 2007). The generally flood-dominant tidal currents are oriented towards the northeast (southwest) during peak flood (ebb) with the minor axis of the tidal ellipsis decreasing from offshore to onshore. The dominant wave direction based on wave statistics is south west followed by waves approaching from west-northwest to north-northwest sector (Vuik et al., 2020). Stormy wave conditions, which drive significant changes in dunes, supratidal beaches (Haerens et al., 2012), and shallow-water morphology, are typically associated with waves originating from the north-northwest sector (Kolokythas et al., 2023). Along the Belgian coast, the seabed is predominantly sandy in the western sector, while finer, cohesive sediments (mixtures of sand and mud) are concentrated in the northeast, particularly within the coastal turbidity maximum near Zeebrugge (Fig. 3). These fine sediments are believed to originate from the paleo-Scheldt River and are redistributed by local hydrodynamics. Their concentration exhibits strong seasonal variability, with higher surface suspended particulate matter during winter months (Adriaens et al., 2018; van Maren et al., 2020).

2.2. Numerical model

2.2.1. Model formulation

The TELEMAC-MASCARET modelling suite (v8.4) consists of several modules to predict coastal, riverine, and estuarine hydro-morphodynamics. Firstly, the TELEMAC2D model solves the non-linear shallow water equations to model the dynamics of the long waves, i.e. in cases when the water depth is much smaller than the wavelength. The depth-averaged equations are solved using the finite element method.

$$\frac{\partial h}{\partial t}+\frac{\partial hU}{\partial x}+\frac{\partial hV}{\partial y}=0 \tag{1}$$

$$\frac{\partial (hU)}{\partial t}+\frac{\partial (hUU)}{\partial x}+\frac{\partial (hUV)}{\partial y}=-gh\frac{\partial Z_s}{\partial x}+\nabla\cdot[h(\nu+\nu_t)\nabla U]+S_x \tag{2}$$

$$\frac{\partial (hV)}{\partial t}+\frac{\partial (hUV)}{\partial x}+\frac{\partial (hVV)}{\partial y}=-gh\frac{\partial Z_s}{\partial y}+\nabla\cdot[h(\nu+\nu_t)\nabla V]+S_y \tag{3}$$

Eqs. (1)–(3) are the mass conservation, and momentum equations in

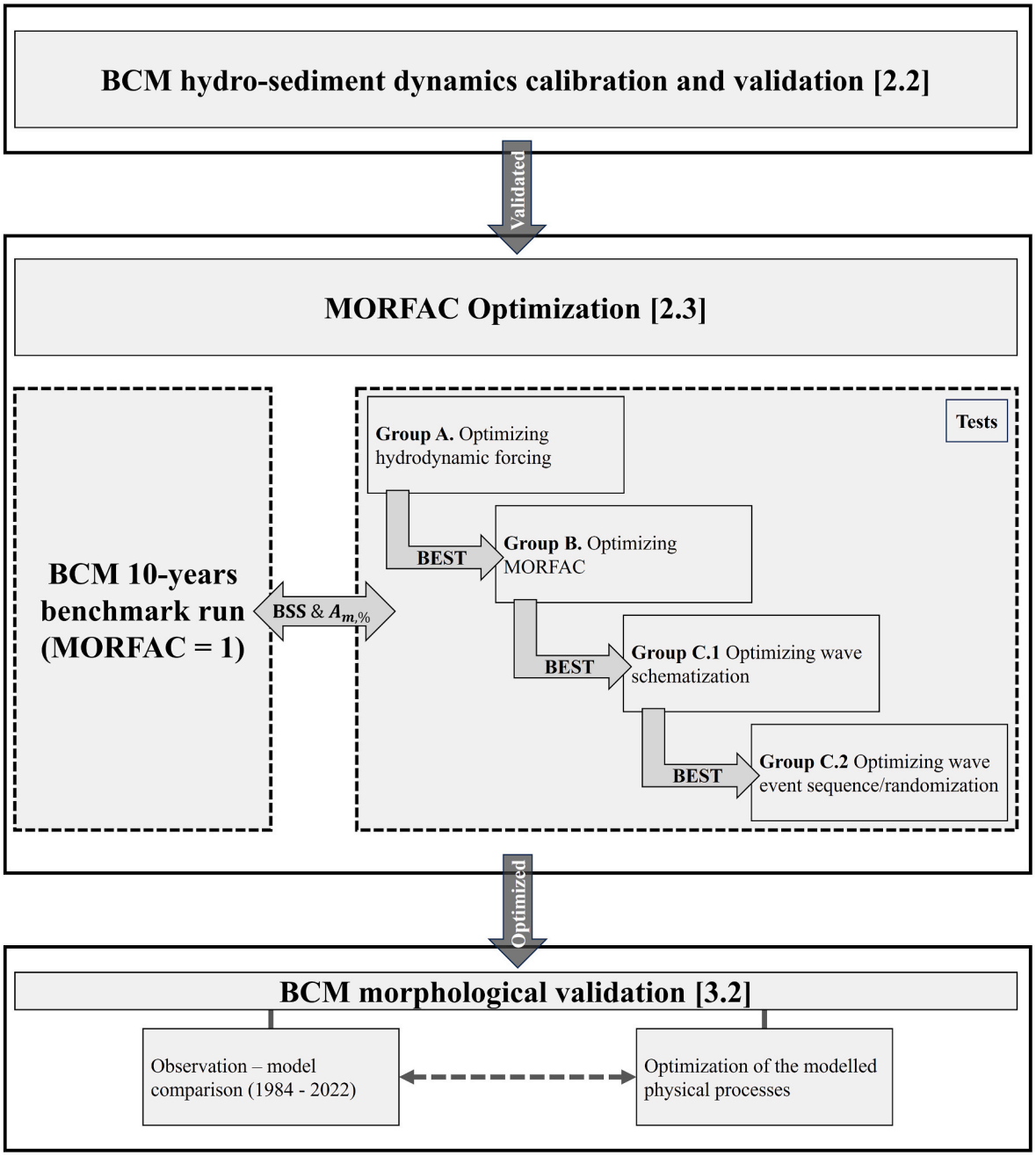

Fig. 2. Research strategy and modelling framework.

x and y directions respectively. Here t is time, h is the total water depth, U and V are the depth averaged velocities in x and y directions, g is the gravitational acceleration constant, Z_s is the free surface elevation, ν and ν_t are the molecular and turbulent viscosities respectively. S_x and S_y represent source and sink terms due to wind, Coriolis, wave forces and bottom friction. To take the turbulence effects into account, the Smagorinsky sub-grid turbulence model was used to determine the value ν_t (Smagorinsky, 1963). The bottom friction is usually a parameter that needs calibration to match the measured free surface and current speeds to their modelled equivalents. However, the friction model accounting for the water depth (Bi and Toorman, 2015) was used to spend less efforts to calibrate the model. Unlike the original implementation, the effects of suspended sediment concentration on flow viscosity were omitted from the present study to avoid numerical instability, as high suspended sediment concentrations in the water column led to unrealistically high viscosity values in intertidal zones.

Secondly, the short wave model TOMAWAC which was coupled with TELEMAC2D, solves the time dependent wave action equation (Eqs. (4)–(6)) to model the temporal and spatial variation of the power spectrum of wind-induced waves in deep, intermediate and shallow waters by using the finite element method.

$$\frac{\partial N}{\partial t}+\dot{x}\frac{\partial N}{\partial x}+\dot{y}\frac{\partial N}{\partial y}+\dot{k_x}\frac{\partial N}{\partial k_x}+\dot{k_y}\frac{\partial N}{\partial k_y}=Q\left(k_x,k_y,x,y,t\right) \tag{4}$$

$$\dot{x}=C_g\frac{k_x}{k}+U \text{ and } \dot{y}=C_g\frac{k_x}{k}+V \tag{5}$$

$$\dot{k_x}=-\frac{\partial\sigma}{\partial h}\frac{\partial h}{\partial x}-\boldsymbol{k}\frac{\partial \boldsymbol{u}}{\partial x} \text{ and } \dot{k_y}=-\frac{\partial\sigma}{\partial h}\frac{\partial h}{\partial y}-\boldsymbol{k}\frac{\partial \boldsymbol{u}}{\partial y} \tag{6}$$

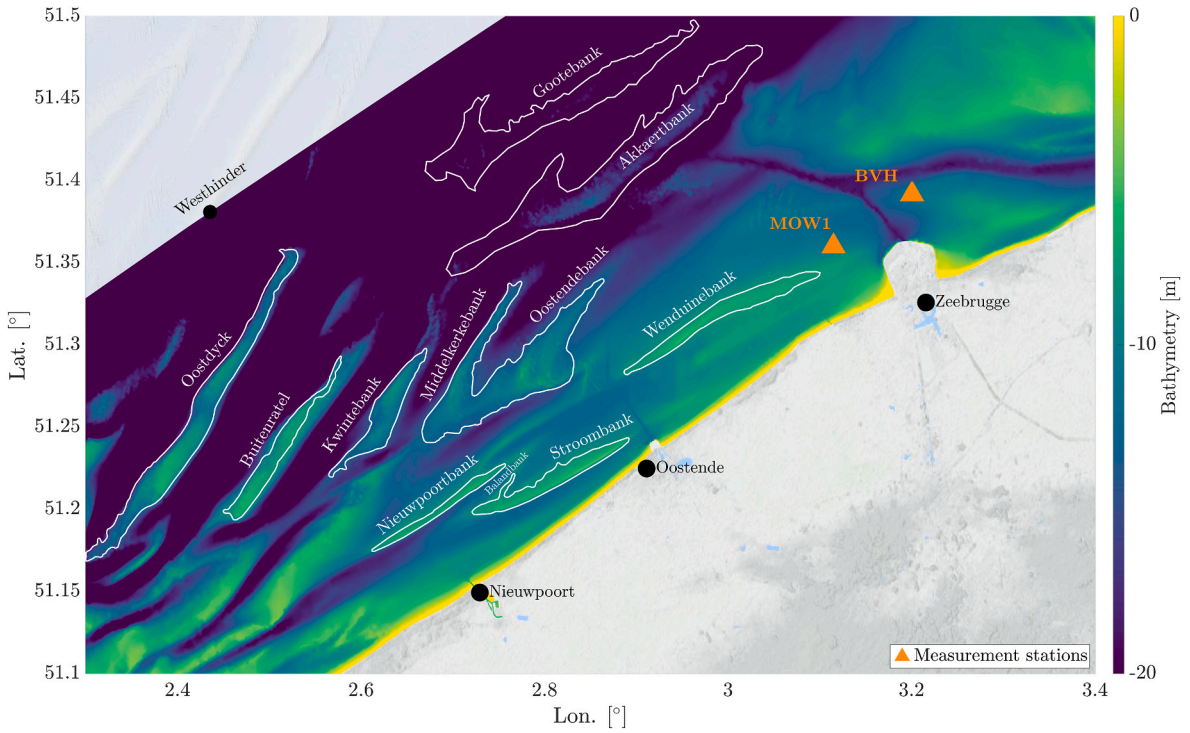

Fig. 3. The Belgian tidal sandbanks within the model domain (Hinderbanks and Thorntonbank are not shown in this figure since they lie outside the model domain). Orange triangles show the locations of the existing measurement stations for model validation; hydrodynamics (BVH) and sediment transport (MOW1). (See Fig. SI–2 and Table SI–1 for the locations and Fig. SI-4-10 for the validation results of additional stations).

In these equations N is the directional spectrum of wave action density, $\dot{x}$, $\dot{y}$ and $\dot{k}_{x,y}$ are the transfer rates in the respective direction, $Q(k_x, k_y, x, y, t)$ is the source-sink term that takes energy transfer from winds to waves, whitecapping, non-linear quadruplet and triad interactions, bottom friction effects, wave breaking effects, enhanced breaking dissipation due to the presence of current, vegetation effects and porous media related dissipation into account, C_g is the group velocity which the wave energy moves at, $\boldsymbol{k}$ is the wave number vector such that $\boldsymbol{k} = k_x\hat{i} + k_y\hat{j}$, σ is the relative angular frequency that obeys the dispersion relation, and $\boldsymbol{u}$ is the current velocity such that $\boldsymbol{u} = U\hat{i} + V\hat{j}$. Since the Belgian nearshore (Fig. 3) is characterized by a gentle sloping seabed, the breaking formulations currently implemented in TOMAWAC produce excessive energy losses, as they assume breakers to behave as fully saturated bores. Initial model tests indicated that this overestimation of breaking-related energy losses leads to an increasing underestimation of wave heights from deeper to shallow zones. In the present study, the depth-induced breaking energy losses were modified using a method that accounts for local bed slope effects in gentle sloping bottom topography (Pezerat et al., 2021). After a thorough comparison between the original wave breaking formulation of Battjes and Janssen (1979) and the modified version proposed by Pezerat et al. (2021), the latter was selected for the rest of the simulations.

For the sediment transport computations and related bed level update, GAIA is coupled online with TELEMAC2D and TOMAWAC (Tassi et al., 2023). Suspended cohesive and non-cohesive sediment transport is solved with the advection and diffusion equation (Eq. (7)):

$$\frac{\partial hC_i}{\partial t} + \frac{\partial hUC_i}{\partial x} + \frac{\partial hVC_i}{\partial y} = \frac{\partial}{\partial x}\left(h\varepsilon_s \frac{\partial C_i}{\partial x}\right) + \frac{\partial}{\partial y}\left(h\varepsilon_s \frac{\partial C_i}{\partial y}\right) + E_i - D_i \tag{7}$$

Where $C_i = C_i(x, y, t)$ is the depth-averaged mass concentration of sediment class i in g/l, U and V are the depth averaged velocity components in x and y directions, respectively, ε_s is the turbulent sediment diffusivity such that $\varepsilon_s = \nu_t/\sigma_c$ where σ_c is the Schmidt number and taken as equal to 1.0, E_i and D_i are the erosion and deposition fluxes of the corresponding sediment class i, respectively.

In this study, the mixed sediment erosion fluxes and critical shear stress for erosion were taken into account by the approach proposed by Le Hir et al. (2011) which is incorporated into GAIA by default. According to this method, if the bed mud mass fraction exceeds 50%, the bed is considered mud. In this regime, the critical erosion shear stress and erosion flux are defined by the mud properties and computed using Partheniades' law (Partheniades, 1965). Conversely, when the mud fraction falls below 30%, the bed is characterized as non-cohesive. Under these conditions, the critical shear stress is set to the sand value, while bedload and erosion fluxes are calculated using the Soulsby-van Rijn formulation (Soulsby, 1997). This formulation assumes a local equilibrium where the sediment transport load instantaneously reaches capacity conditions. We consider the Soulsby–van Rijn equation the appropriate choice to predict sediment transport through the combined action of waves and currents. For intermediate mud fractions (30-50%), the mixed-sediment erosion flux and critical shear stress are obtained by linearly interpolating between the erosion characteristics of the individual sediment classes. The depth-averaged suspended transport equation (Eq. (7)) accounts for suspension capacity through a theoretical closure for the critical shear stress for deposition, which is derived from suspension capacity theory by Toorman (2000), that was first implemented into TELEMAC by Bi and Toorman (2015). Furthermore, the active layer concept (Hirano, 1971) with a 0.05 m layer thickness is used to limit the availability of sediments that can be mobilized to avoid overestimation of bed erosion. While the sediment transport formulation described here represents a specific configuration, the MORFAC optimization procedure detailed in Section 2.3 remains applicable for any sediment transport equation set.

In GAIA, morphological evolution is modelled using the Exner equation which solves the sediment bed mass conservation (Eq. (8)). In this equation, λ is the sediment porosity which is equal to 0.4, z_b is the bed elevation above datum (m), ρ_s is the sediment density (kg m^{-3}), $\boldsymbol{Q_{mb}}$ is the vector of dry mass transport rate per unit width without pores (kg

$m^{-1}\ s^{-1}$), *MORFAC* is the morphological acceleration factor, D and E are the deposition and erosion fluxes (kg $m^{-2}\ s^{-1}$), respectively.

$$(1-\lambda)\frac{\partial(\rho_b z_b)}{\partial t}+\nabla\cdot\boldsymbol{Q_{mb}}=MORFAC\times(D-E) \quad (8)$$

2.2.2. The Belgian Coast Model (BCM)

In this study we used an online coupling of the depth-average flow module TELEMAC2D, the wave-module TOMAWAC and the sediment transport/morphodynamics module GAIA. The resulting coupled model is able to predict the impact of tides, storm surges and waves on coastal sediment transport and morphodynamics. To achieve realistic boundary and hydrodynamic conditions in the Belgian coastal zone, we employed a nesting approach following Escobar et al. (2023). A coarse resolution hydrodynamic model of the entire North Sea (further referred to as North Sea Model, NSM) couples flow (TELEMAC2D) and waves (TOMAWAC). The flow model is forced by all tidal constituents available in the TPXO9 database (Egbert and Erofeeva, 2002). The NSM uses the spatially and temporally varying wind field from the ERA5 1.0° resolution-hourly 10-m data product (Hersbach et al., 2020) to generate wind-induced currents and short waves. The high resolution hydro-morphodynamic Belgian Coast Model (BCM), integrating flow (TELEMAC2D), waves (TOMAWAC), and morphodynamics (GAIA), is nested within the NSM. The nesting is realized by using the NSM to provide boundary conditions to the BCM, including free surface elevation and flow velocity for TELEMAC2D, and a wave spectrum covering 12 directional and 25 frequency bins for TOMAWAC.

The limits of the BCM stretch from Calais (France) to the Dutch Coast including the Western and Eastern Scheldt estuaries. The proposed model shares the similar spatial extents as the model proposed by Kolokythas et al. (2021) with the exclusion of schematized Western Scheldt upstream (Fig. 1b). The BCM covers an area that is roughly 250 × 50 km in longshore and cross-shore directions, respectively. The coupling between TELEMAC2D and TOMAWAC was performed with the TEL2TOM approach (Breugem et al., 2019) eliminating the requirement of having identical meshes for TELEMAC2D and TOMAWAC which allowed for substantial reduction in the computational time. Both meshes were generated using GMSH (Geuzaine and Remacle, 2009). In the offshore area the mesh resolution was defined inversely proportional to the local bottom slope. In the area of interest (Fig. 3), between Nieuwpoort and Oostende, the TELEMAC2D (TOMAWAC) mesh size was refined to 100 m (400 m). This refinement was needed to represent the Nieuwpoortbank and Stroombank (Fig. 3) dimensions accurately, for which the morphological validation was performed. The resultant mesh (Fig. 1b) for TELEMAC2D (TOMAWAC) has 137 802 (21 472) nodes and the mesh size varies between 25 and 1000m (100-1400m). The model time-step was set to 15s (300s) for TELEMAC2D (TOMAWAC) and the wave and flow models were coupled every 600s. While larger time steps and mesh sizes yielded similar hydrodynamics, the present configuration produced more accurate suspended particulate matter (SPM) values compared to the field measurements as finer mesh captured the bottom and stratigraphical gradients more accurately by reducing the uncertainty related to the mesh interpolation to which the SPM was more sensitive. Following a parallel efficiency analysis to optimize computational cost, the model was run using 42 cores on Intel Xeon Platinum 8360Y CPUs (2.4 GHz) to reduce computational time.

The model bathymetry is composed of two different sources: (i) the bathymetry data for the North Sea was obtained from GEBCO Database (GEBCO Compilation Group, 2020), (ii) the bathymetry for the near coastal zone collected by the French, Belgian and Dutch authorities and compiled by Kolokythas et al. (2021) was utilized for the region closer to Belgium, and parts of the French and Dutch coasts. The latter was utilized for the hydro-sediment predictions and the *MORFAC* optimization performed with the BCM. To keep computational time manageable across multiple tests, coastal structures (e.g., groins and breakwaters) were excluded, as accurately resolving these features requires a grid resolution significantly finer than 100 m. For example, Kolokythas et al. (2021) used a 25 m mesh to resolve the Belgian Coast morphodynamics with coastal structures included, which resulted in nearly double the number of nodes compared to this study. Additionally, dredging and dumping were not included due to a lack of data for the long-term simulation. The initial mud content (bed material <63 μm) in the BCM varied spatially and was compiled from different sources (Fig. SI–3): for the offshore sector, the survey results from Van Lancker et al. (2007) were utilized; for the Western Scheldt, the maps published by Eck (1999) were digitized; and for the offshore part of the Netherlands and the Eastern Scheldt, the data obtained from SHOM (2021) was used. The bed was discretized into four vertical layers, referred to as, from top to bottom, layers 1 to 4. The upper layer represents the easily erodible fluffy mud layer which was mainly confined near the region around Port of Zeebrugge and has an initial thickness of 0.5 m (Van Maren et al., 2020) (Fig. SI–3). The thicknesses of the lower three layers, namely Upper Holocene, Lower Holocene and Pleistocene, varied spatially based on the 3D Voxel model for the BPNS proposed by Hademenos et al. (2019). The thicknesses of the remaining parts that are outside the BPNS were initially set to 0.5 m and 1.5 m for the Upper-Lower Holocene and Pleistocene layers, respectively, based on Bi and Toorman (2015). The Lower Holocene layer represents tidal flat environments only present in the nearshore area and submerged around 7 500 cal BP, including coarse-grained to very-fine sand. The Upper Holocene covers the entire Belgian Continental Shelf and consists of fine sands related to an estuarine-marine environment in the nearshore area, and medium to coarse sand further offshore (Hademenos et al., 2019). The Pleistocene layer reflects the older, compacted and harder to erode bed material. To reduce the impact of uncertainties and discontinuities in the initial data, the model was run for one year (year 2012) to smooth the spatially discontinuous bathymetry and stratigraphy until the equilibrium between hydrodynamics, sediment transport and morphology was established.

The BCM predicts transport of two sediment classes: non-cohesive sand (d_{50} = 300 μm) and cohesive mud (d_{50} = 60 μm). The process of flocculation was not explicitly accounted for in the current model. Values for the settling velocities of sand and mud (0.045 m/s and 0.003 m/s, respectively), critical shear stress for mud erosion ($\tau_{cr,m}$), mud concentration and erosion rate constant of the layers (E) (Table 1) were used to calibrate the sediment transport model based on the SPM data collected by Fettweis et al. (2016) at MOW1 station (Fig. 3). The increase of $\tau_{cr,m}$ and mud concentration per layer related to bed stratification (fluffy, upper & lower Holocene and Pleistocene) represents the presence of consolidated layers with reduced erodibility.

2.2.3. Hydrodynamic and sediment transport performance of the BCM (2013)

The hydrodynamic performance of the present model was evaluated for year 2013, after conducting a one year spin-up period (year 2012). Model predictions on free surface elevation, current velocity, wave height, wave period and wave direction were compared with observational data from https://www.meetnetvlaamsebanken.be for the observation piles and wave buoys presented in Fig. SI–2 (four measuring piles for TELEMAC2D, seven wave buoys for TOMAWAC). The year 2013 was selected because it included a major storm event, Xaver locally also called “Sinterklaasstorm”, which produced the highest water levels since the infamous storm of 1953 (Montreuil et al., 2015). This, therefore, allowed an assessment of the model performance under both calm and storm conditions. As all relevant hydrodynamic quantities were recorded at the Bol van Heist (BVH) station during the Sinterklaasstorm, the results are presented for BVH in the main text (Fig. 3). Data from other stations, along with their plots, coordinates, and abbreviations, were provided in the supplementary material (Fig. SI–2 and Table SI–1).

The free surface elevation, depth averaged current speed and direction, spectral wave height, spectral wave period, and mean wave direction at the BVH station are shown as an example of model the

Table 1
Stratigraphic properties defined in the model.

#	Layer	$\tau_{cr,m}$ [Pa]	Mud concentration of the layers [g/L]	E [$kg/m^2/s$]	Initial Thickness [m]	
					BPNS	Other
1	Fluffy	0.5	250	8×10^{-4}	0.5 m	
2-3	Upper & Lower Holocene	1.2	500	8×10^{-4}	3D Voxel	0.5
4	Pleistocene	2.5	750	8×10^{-4}	3D Voxel	1.5

performance (Fig. 4a–f, see Fig. SI-4-10 for additional results). The coefficient of determination (R^2) for the entire year of 2013 range from 73.12% to 98% for water level and current velocity. However, there is a slight mismatch between observed and modelled water levels and current velocities that can be attributed to several sources of uncertainty. First, uncertainties in the initial bathymetry, compiled from various data

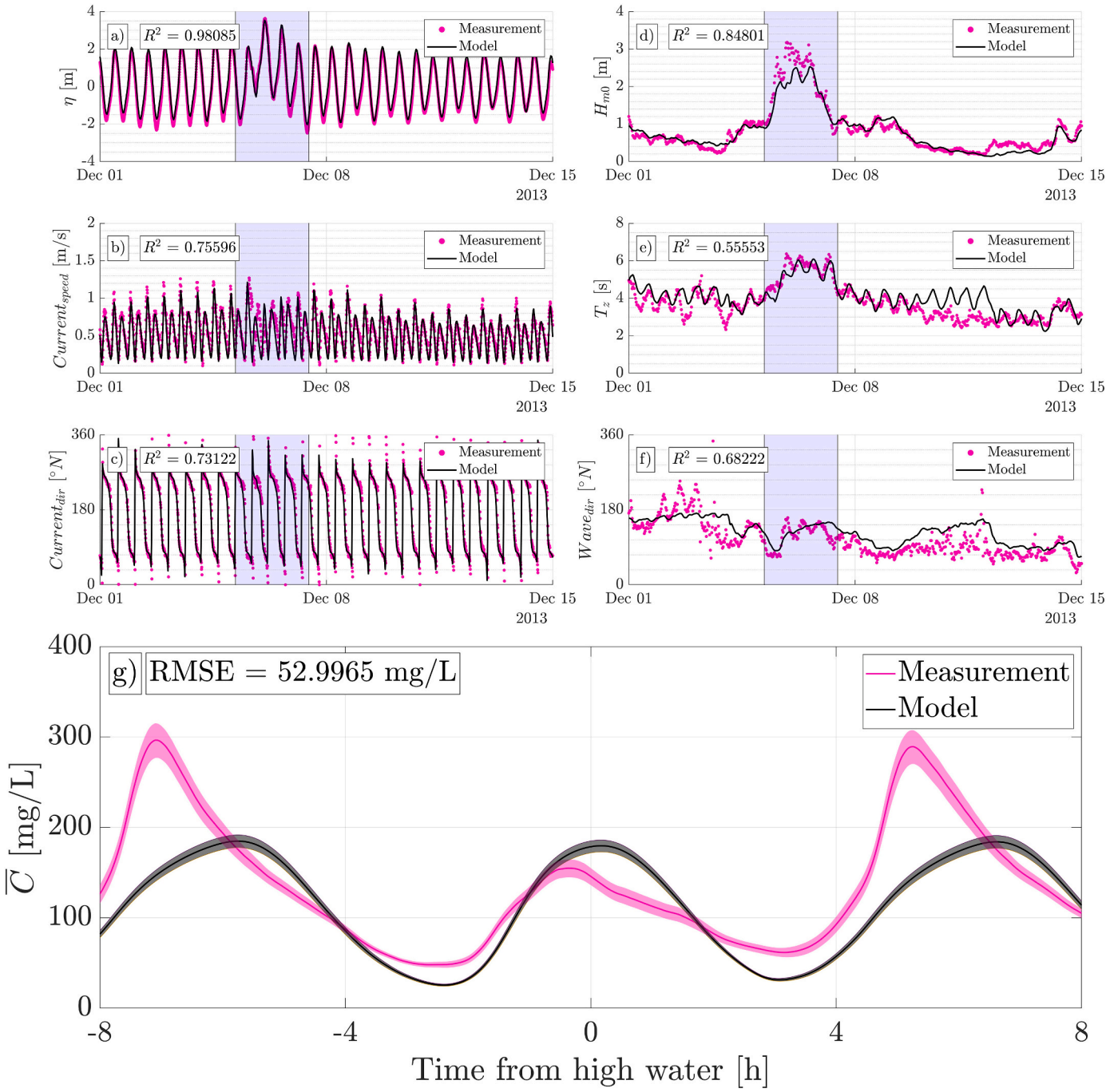

Fig. 4. Validation of (a) free surface elevation, (b) current speed, (c) current direction, (d) wave height, (e) wave period, (f) wave direction at Bol van Heist station, (g) ensemble averaged SPM at MOW1 station. Shaded blue zone in (a-f) highlights the Sinterklaas storm R^2 values in (a-f) and *RMSE* value in (g) are computed for the entire 2013.

sources collected in different years, affect tidal propagation, as the modelled bathymetry deviates from the actual bed morphology. Furthermore, anthropogenic interventions such as dredging, dumping, and coastal structures being not accounted for in the model alter the actual morphology compared to the bathymetry used in the model. Second uncertainty arises from the model formulation itself. More specifically, the used depth-averaged model, may be misrepresenting flow patterns at some locations e.g. the BVH station where three-dimensional transport phenomena are crucial.

The wave model results are in acceptable agreement with the measured data with respect to wave height, period and direction, during both calm and storm conditions (Fig. 4d–f). The R^2 values for these quantities range from 55.5% to 84.8%. On the other hand, high-energy events are underestimated by 20% on average. Comparatively lower performance of the wave model likely stems from the large-scale NSM, which supplies spatio-temporally varying boundary conditions for the BCM. The NSM uses ERA5 hourly wind reanalysis data (Hersbach et al., 2020) for the computation of the wind source term in Eq. (4) to drive the large-scale wave field across the North Sea, which is highly sensitive to wind forcing. Wang et al. (2021) reported that ERA5 database underestimate wind speeds at Westhinder station by up to 25%. This underestimation translates to lower wave heights in the NSM, which are subsequently inherited by the BCM wave model via nesting. Overall, the hydrodynamic model performs relatively good compared to the available studies for the region of interest (e.g., Bi and Toorman, 2015; Escobar et al., 2023; Kolokythas et al., 2021; Wang et al., 2021). It demonstrates its ability to capture dominant processes, namely, astronomical tidal variations, wind-induced waves, surges and currents both during storms (shaded blue area on the plots) and calm periods.

The performance of the sediment transport model GAIA was evaluated by comparing the modelled depth-averaged sediment concentration with in-situ SPM measurements from station MOW1 (Fettweis et al., 2016) (Fig. SI–2). At MOW1, sediment concentrations were measured at two heights in the water column and must be converted to depth-averaged values for model comparison. This conversion was performed using a Rouse profile (Eq. (9)), with the Rouse number, b, fitted from the two observations: the reference concentration, $C_a(z_a = 0.2\ m)$, at level, $z_a = 0.2\ m$ above the bed; and concentration at level $z = 2.0\ m$ given by $C(z = 2.0\ m)$. The water depth, h, at MOW1 was taken from the hydrodynamically validated model. The fitted b was then applied in Eq. (10) to integrate the profile over depth and to obtain the corresponding depth-averaged SPM.

$$C(z) = C_a\left(\frac{z_a}{z}\frac{h-z}{h-z_a}\right)^{-b} \tag{9}$$

$$\overline{C} = \frac{\int_{z_a}^{h} C(z)dz}{h} = \frac{\int_{z_a}^{h} C_a\left(\frac{z_a}{z}\frac{h-z}{h-z_a}\right)^{-b} dz}{h} \tag{10}$$

A comparison between the modelled depth-and-ensemble-averaged SPM concentration and measured data shows that the model is capable of reproducing the correct magnitudes of depth-averaged SPM concentrations at the MOW1 station during ebb and flood (Fig. 4g). While the model successfully captures the overall SPM dynamics, some differences remain in the exact phase and magnitude of the ensemble-averaged results. Such deviations are common in depth-averaged mixed sediment transport models due to several reasons. First, the model does not account for flocculation dynamics explicitly, which are particularly important at the location of interest (MOW1) for the time series analysis (Escobar et al., 2023). Reproducing detailed flocculation dynamics, especially those governed by organic matter and phytoplankton (Shen et al., 2018), goes beyond the scope of the current study. Incorporating such processes could potentially improve predictions but would also introduce additional sources of uncertainty. Second, unlike the present modelling strategy, SPM measurements capture not only suspended sediments with a continuous size distribution but also other particulate matter, such as organic material which could also influence bed erosion characteristics (Van Maren et al., 2020). Third, SPM collected at 0.2 m and 2.0 m above the bed had to be converted to depth-averaged concentrations assuming a Rouse profile, which is strictly only valid under steady, uniform conditions. The validity of this assumption over the entire time series remains unclear. Despite these uncertainties, the model performs well compared to previous studies modelling SPM concentrations at the MOW1 station (Bi and Toorman, 2015; Escobar et al., 2023; Van Maren et al., 2020).

2.3. MORFAC optimization

The following section outlines the optimization strategy for morphological predictions using the MORFAC method. The validated model was first applied to perform an 11-year morphological simulation (2012-2023), using 2012 as a spin-up period and 2013-2023 as the benchmark run. This reference simulation, conducted with a morphological acceleration factor (*MORFAC*) of 1 and forced by the "real" flow and wave boundary conditions generated by the NSM, served as the baseline for comparison. The optimization strategy for the MORFAC method involves the systematic modification of three key components (Fig. 2), thus dividing the model tests into three distinct groups (Group A, B, C). Group A focuses on the discretization of hydrodynamical boundary conditions, examining whether it is preferable to use real or representative tides, with or without synthetic wave conditions, combined with or without generated synthetic storm surges following Pineau-Guillou et al. (2023). Results from this analysis were used to determine the optimal boundary condition setup for subsequent model runs. Group B evaluates the model's predictive performance in response to the selected *MORFAC* values under calm and storm conditions. Group C assesses the influence of assumptions made during the construction of the synthetic wave time series on model predictions. Specifically, we evaluated the effects of the number of schematized conditions (including the separation of storm and calm conditions) used to generate the synthetic wave time series, the exclusion of waves exiting the domain, event sequencing, and event randomization on model performance.

To balance model accuracy and computational efficiency, the (weighted) Brier Skill Score (BSS) (Sutherland et al., 2004) (Eq. (11)) and area percentage of matching erosion/deposition processes ($A_{m,\%}$) (Eq. (12)) were used as metrics. The former provides a quantitative information on the morphological evolution while the latter gives an estimation of the pattern prediction or qualitative accuracy.

$$BSS = 1 - \frac{\sum_{j=1}^{n} w_j\left(\Delta Z_{j,MORFAC} - \Delta Z_{j,Ref}\right)^2}{\sum_{j=1}^{n} w_j\left(\Delta Z_{j,Ref}\right)^2} \tag{11}$$

In Eq. (11), ΔZ_j is the bed level difference between the final and initial bathymetries for node j out of n number of nodes, and subscripts *MORFAC* and *Ref* represents the accelerated and benchmark simulation results, respectively. Since the model grid is unstructured, each node is given a weight, w_j, proportional to the Voronoi area it occupies. The model performance can be classified by the *BSS* ranges provided in Table SI–2.

$$A_{m,\%} = \frac{\sum_{j=1}^{n} Match_j}{n} \times 100 \tag{12}$$

In Eq. (12), $Match_j$ is a factor inidcating whether the accelerated model could produce the same process (erosion or deposition) as the reference model. For the former, $Match_j$ was set equal to 1, where for the latter it is set to 0. Apart from scoring, the same algorithm was used to identify whether the accelerated model produces false erosion, $A_{fe,\%}$, (reference

→ deposition, accelerated → erosion) or false deposition, $A_{fd,\%}$ (reference → erosion, accelerated → deposition) patterns. As a result of the hierarchical optimization tests, a single model producing the highest scores was selected to hindcast the morphological evolution of the Belgian Coast between 1984 and 2022 around the region between Nieuwpoort and Oostende. A summary of all group-test configurations is provided in Table SI–3. Below, we present an overview of the conducted tests together with the rationale for the selected tests and their sequence.

2.3.1. Group A: hydrodynamical discretization

Tides. Previous studies utilized morphological upscaling (using the MORFAC method) by using real tides (i.e. dominant tidal constituents) to capture natural variability or representative tidal cycles to simplify boundary conditions and to reduce computational demands (e.g. de Vriend et al., 1993a; Latteux, 1995; Schrijvershof et al., 2023; Steijn, 1992, 1989; Winter, 2007). Since the Belgian coastal zone is influenced by waves, tides, and storm surges, it is crucial to carefully examine how variations in each factor, as well as their interactions, affect morphological predictions. The present study investigated two different spatially varying tidal boundary conditions both of which were generated by the larger scale NSM. The first configuration did not apply any simplification to the tides and includes spring-neap variations. The second option used the tidal elevations and velocities, modelled by the NSM from 25 to 05-2014 17:20 to 26-05-2014 18:10 as a representative tide which could reproduce the mean sediment transport quantities during 2014 according to Kolokythas et al. (2023), and which was repeated at the model boundary throughout the simulation.

Waves. The stochastic nature of the wave climate makes it challenging to reproduce the morphological impact of realistic wave condition sequences in long-term simulations (De Vriend et al., 1993a). To overcome this limitation, synthetic wave time series can be constructed from schematized representative wave conditions based on observed wave statistics. This approach enables systematic testing of the influence of wave sequence and variability on model outcomes. Wave schematization was performed using wave data collected between 2013 and 2023 at the Westhinder wave buoy (Fig. 3), following the wave energy flux concept (Roelvink et al., 2018). This approach was shown to be successful in previous studies (Roelvink et al., 2018); however, it remains unclear whether the separation of storm and non-storm conditions is necessary, and if so, how such a separation should be implemented most accurately. The wave energy flux concept divides the dataset into wave height and directional bins such that each bin contains an equal amount of wave energy. To generate such a synthetic wave time series, 12 calm and 6 storm conditions covering the directions from 0° to 360°N, along with their associated probabilities, were used to randomly assemble the wave sequence. A threshold of $H_{m0} \geq 3.0\ m$ was applied to classify data as storm conditions (Fig. 5a). The schematization was carried out independently for storm and calm conditions, ensuring that each bin within its group (storm or calm) contained equal wave energy. During calm periods, the wave boundary condition was held constant for one day and then transitioned smoothly over 10 min to the next condition. Storm durations were limited to a maximum of 1.5 days, during which the *MORFAC* value was reduced to 1.0. Throughout the first group of tests, this same synthetic wave boundary condition was applied whenever wave forcing was included. Tests excluding the waves from the model were used to evaluate the importance of the waves on the accurate modelling of the long-term morphological changes.

Storm surge. Due to their intermittent occurrence, the impact of storm surges on morphological development is difficult to predict (Matheen et al., 2021). Therefore, we tested the effect of synthetic storm surges on the model results. The storm surge schematization was based on the storm surge height extracted from the Westhinder measuring station. We carried out a tidal fit computed with the MATLAB tool T_TIDE proposed by Pawlowicz et al. (2002) and subtracted it from the measured signal. Then, these residual data were used to generate the schematized storm surge by the method proposed by Pineau-Guillou et al. (2023). The resultant schematized surge time-series is given by Fig. 5b. The spatially non-varying schematized surge was superposed to a spatially varying tide at the model boundary for the relevant tests. If the wave schematization of the relevant tests distinguishes the storm and calm conditions, then the same surge peak occurs in the middle of the storm regardless of the storm direction (Fig. 5c).

2.3.2. Group B: MORFAC value

In addition to the forcing schematization, the sensitivity of the present model performance to the magnitude of the *MORFAC* values was investigated. Roelvink (2006) suggested that the critical *MORFAC* is reached before the model stops capturing the essential interaction between flow and morphology. However, this is difficult to assess in large-scale simulations. Therefore, model predictions of bed level

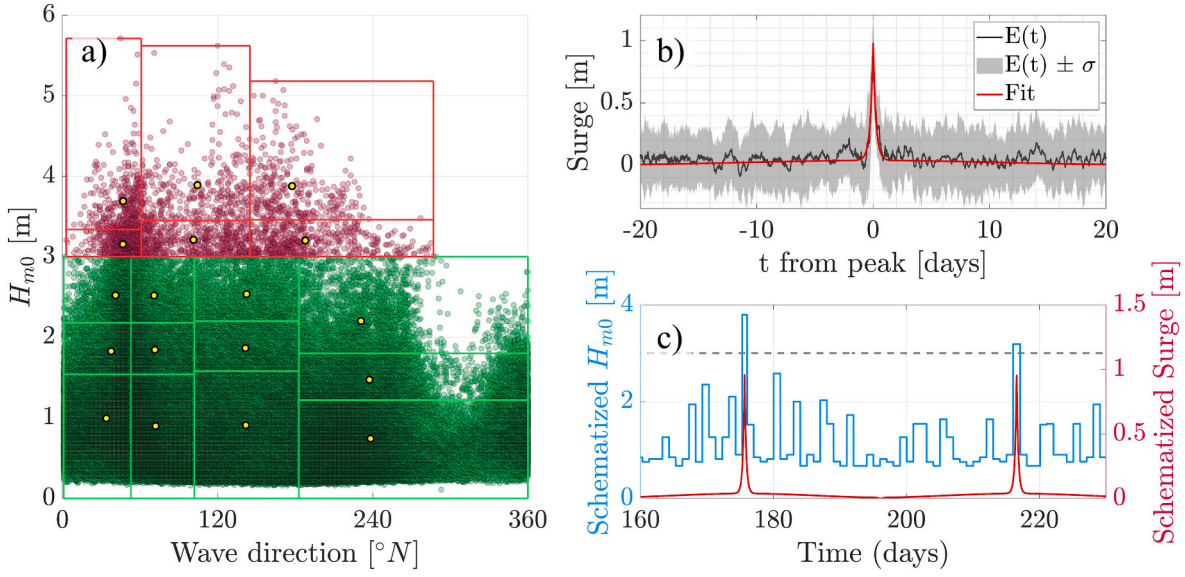

Fig. 5. An example of (a) wave (red for storm, green for calm conditions) and (b) storm surge schematization based on the measured data collected at the Westhinder station between 2013 and 2023, used to generate (c) the synthetic wave and surge boundary conditions. Wave direction follows the nautical convention (0°N wave direction represents the waves attacking towards north).

changes were compared to a benchmark simulation to assess the maximum permissible value. For these tests, different values and combinations of *MORFAC* during calm ($MORFAC_{calm}$ 10, 30, and 50) and storm conditions ($MORFAC_{storm}$ 1, 10, 30, and 50) were tested (Table SI–3). To evaluate computational performance, a speed-up factor (S, Eq. (13)) was used.

$$S = \frac{t_{ref}}{t_{MORFAC}} \tag{13}$$

In this equation, t_{ref} and t_{MORFAC} are the computational time (CPU time onwards) to complete the reference and an accelerated model run. If the difference in *BSS* between distinct *MORFAC* value tests is less than 5%, then the test producing a higher S is considered as the most efficient.

2.3.3. Group C: synthetic wave time series

From a morphological viewpoint, morphodynamical predictions are not only shaped by the magnitude and occurrence of forcing factors; their number and sequence also matters. In the final set of tests, the wave boundary condition, previously kept equal in each test, was further refined to produce the most representative wave conditions. Similar to the earlier tests, the schematized wave conditions and their associated occurrence probabilities were used to generate randomized synthetic time series at the boundary e.g., Fig. 5. The Group C tests were categorized into two subgroups. Under the Group C.1 tests, we generated different synthetic wave time series used as the wave boundary condition, with different numbers of schematized wave conditions and directional limits. On the other hand, Group C.2 investigated the morphological impact of event sequences and the randomization of the number of occurrences for each condition to generate the synthetic wave time series. The event sequence tests examined the impact of an event sequence by rearranging the order of fixed number of wave conditions used in the time series for Group A, B, and C.1, generating 9 different time series where the sequence was the only variable. In the randomization test, synthetic time series were generated using the same probability distribution but with different random seeds for selection and sequencing. As a result, while the same probability distribution was used, the number of occurrences for each condition varied slightly due to the random selection, producing 14 additional time series. Group C.2 was therefore composed of 23 different test cases.

Since water level variations strongly influence wave transformation and sediment transport, identical wave boundary conditions might generate different morphological responses depending on the tidal stage at the time of wave forcing. To understand the influence of timing between different forcing on morphological predictions, we need to quantify the alignment between the tidal phase (spring or neap) and wave forcing. For this purpose, first, a tidal modulation coefficient, μ (Eq. (14)), was developed to reflect the timing of the spring and neap tides. This coefficient was computed at the model boundary close to Westhinder, to minimize the uncertainties due to the evolving morphology inside the domain within different tests.

$$\mu(t) = \frac{R(t)}{R_{max}} \tag{14}$$

Where $R(t)$ is the modelled tidal range per cycle time series and R_{max} is the maximum modelled tidal range during the accelerated model run. Throughout the accelerated model runs, μ varied between 0.45 and 1.0 for the neap and spring tides, respectively. Additionally, we also computed the normalized wave energy time series, $E_n(t)$, for each test by Eq. (15).

$$E_n(t) = \frac{[H_{m0}(t)]^2}{H_{m0,max}^2} \tag{15}$$

Where $H_{m0}(t)$ is the synthetic time series of the spectral wave height forced at the model boundary and $H_{m0,max}$ is the maximum value of this time series. Finally, two resultant time series, $\mu(t)$ and $E_n(t)$, were multiplied pointwise to produce a new time series. The mean of this product, denoted as γ (Eq. (16)), quantifies the tendency of higher wave energy events to coincide with either high or low tidal ranges at the boundary. A higher γ value indicates that energetic wave conditions predominantly occur during larger tidal ranges, when low water levels are at their minimum, therefore enhancing the impact of waves on sediment transport and morphological changes.

$$\gamma = \overline{\mu \times E_n} \tag{16}$$

The accelerated model for each test that best represented the reference morphological changes, in terms of *BSS* and $A_{m,\%}$, while providing a reasonable speed-up factor S, was selected for the next set of tests. Even though the final similation outcome was path-dependent, as it was influenced by the selection of the test group sequence, the computational demands of the model required the performance analyses to be conducted sequentially without cross-group testing. The details of all the tests conducted along with their morphological performance for the first group can be found in Table SI–3.

3. Results

3.1. MORFAC optimization

Morphological changes between 2013 and 2023 predicted by the benchmark model, completed in approximately 10.5 days, reveal a general trend of bed migration aligned with the dominant tidal current direction (towards the Northeast) (Fig. 6a, black arrows). In addition, cross-shore movement of tidal sand banks is observed, including the Nieuwpoortbank and the Stroombank. The Nieuwpoortbank migrates towards the coast in a southeast direction (Fig. 6a, magenta arrows), whereas the Stroombank is predicted to migrate offshore to the northeast (light blue arrows).

3.1.1. Group A: hydrodynamical discretization

The Group A tests (Fig. 7a) demonstrate that including waves into the model markedly improves its performance. More specifically, the inclusion of waves increases the BSS from 0.729 to 0.883 under real-tide conditions and from 0.641 to 0.848 under representative-tides. When comparing the impact of real-tide and representative-tides on morphological performance, the real-tide conditions consistently produced better performance of the accelerated model predictions: the *BSS* increased from 0.847 to 0.883 (with waves included), and from 0.641 to 0.729 (with waves excluded). The real tide approach does not affect $A_{m,\%}$ significantly compared to the representative tide approach (Fig. 7a). Our model tests indicate that the synthetic storm surge signal only plays a minor role in improving morphological predictions. Based on the results of Group A test, the model configuration using schematized waves, realistic astronomical tides, and no surge as boundary conditions show the best correspondence to the benchmark case and was selected for the Group B tests.

3.1.2. Group B: MORFAC value

The sensitivity of the model prediction to the magnitude of the chosen *MORFAC* value reveals that lower values such as 10 and 30 show comparable results, while a *MORFAC* of 50 leads to poorer predictions (Fig. 7b), regardless of using different *MORFAC* values during storm ($MORFAC_{storm}$) and calm conditions ($MORFAC_{calm}$). When $MORFAC_{calm}$ is high (50), increasing $MORFAC_{storm}$ from 1 to 50 raises *BSS* drastically from 0.781 to 0.849 (+8.7%). With lower $MORFAC_{calm}$ (10-30), increasing $MORFAC_{storm}$ from 1 to 30 increases *BSS* from 0.861 to 0.893 (+3.5%). Since the difference between the two best-performing models, which are $MORFAC_{calm,storm} = 10$ and 30, is less than 5% (*BSS* equal to 0.912 and 0.893, respectively) a *MORFAC* value of 30 for both calm and storm conditions is selected to balance accuracy and computational cost

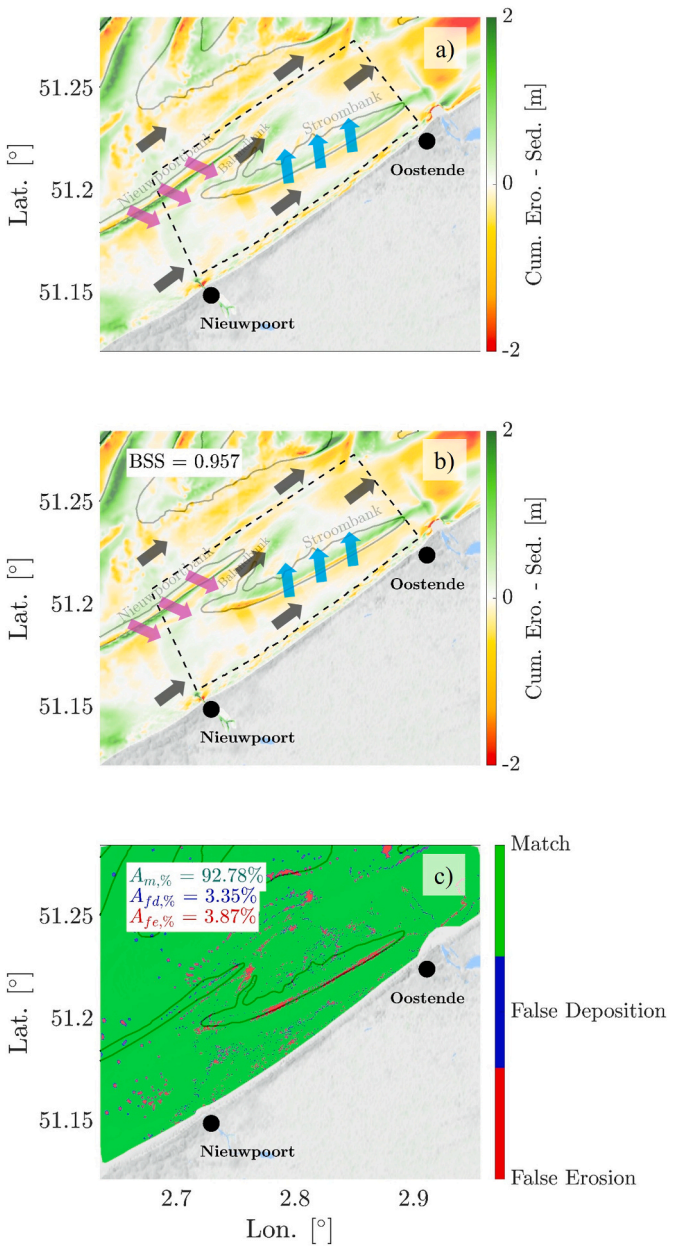

Fig. 6. Cumulative sedimentation and erosion map computed for 2013-2023 by the (a) reference model and (b) the best-performing accelerated model. (c) Erosion-deposition match map when comparing (a) and (b). Arrows show bedform migration of Stroombank (light blue) and Nieuwpoortbank (magenta) directions computed by the models. Overlay map was obtained through EMODnet [https://emodnet.ec.europa.eu/].

($S = 27.2$), and is carried forward into Group C testing.

3.1.3. Group C: synthetic wave time series

Group C.1 test results suggest that the separation of storm and calm conditions during wave schematization has a negative impact on the predictive performance (Fig. 7c, green-red symbols), while uniform schematization produces more accurate morphological predictions (Fig. 7c, blue symbols). It is observed that an increased number of wave conditions does not always result in a better *BSS*. Moreover, morphological performance was further improved by excluding waves propagating out of the domain (Fig. 7c, coverage 45-240 °N). Wave conditions providing the highest model skill were retained for the Group C.2. More specifically, 12 different conditions were discretized, covering the directions between $45 - 240°N$, and excluding waves propagating out of the domain.

The results of the Group C.2 (Fig. 7d) show how sensitive the morphological results are to the event sequence and the randomization of the synthetic wave time series in the accelerated model. More specifically, variations in event sequence and randomization can lead to similar improvement/decrease in model skill observed in previous tests of Groups A to C1 (Fig. 7a–c). This range of variation is attributed to the simultaneous occurrence of higher-energy wave conditions at relatively lower water levels during spring tides. This was verified by comparing the model performance (BSS) to the co-occurrence of high energy wave events and spring tides (γ) at the model boundary (Fig. 8). Model performance increases consistently with increasing γ up to γ_{ref} (γ-factor of the benchmark model) (see Section 4.1 for the computation of γ_{ref}). Tests conducted with $\gamma > \gamma_{ref}$ showed reduced model performance, indicating the existence of an optimal γ-factor linked to γ_{ref}.

3.2. Model application on predicting the multi-decadal morphological evolution of the Belgian Coast

The optimized model configuration of the accelerated model was: (i) real tides, (ii) synthetic wave time series constructed with schematized wave conditions generated using only those entering the domain with 12 conditions and without any separation between storms and calms, and (iii) without synthetic storm surge. The proposed wave boundary condition was further optimized in the randomization test by quantifying the co-occurrence between waves and tides (Figs. 7d and 8) resulting in 'Excellent' quantitative performance ($BSS = 0.957$) compared to the benchmark run (Fig. 6b and c). This model was used to hindcast the Belgian Coastal evolution between 1984 and 2022 (38 years) provided by Dujardin et al. (2023) as a model application. Data from 1984 was fed into the optimized model as an initial bathymetry and the area outside of this dataset was filled with the bathymetric data from Kolokythas et al. (2021). The small gap between the two datasets was filled using inverse distance interpolation to ensure a smooth transition in the bathymetry and avoid abrupt changes. The accelerated model was run for 38 morphological years, and the performance of the final model was compared to the bathymetry data collected in 2022 for the area that had less direct human impact. The onshore extent of the comparison area was defined to be the −5 m MSL contour. It was extended in the offshore where the mesh size started to become larger than 100 m to avoid resolution related deviations. Western and eastern lateral extents were selected to be confined by the Yzer river outlet in Nieuwpoort and the present-day navigation channel of the Port of Ostend to avoid the mismatch due to the lack of river discharge and dredging of the navigation channel in the model implementation. Different from the optimization study, wave data recorded at the Westhinder buoy between 1995 and 2024 were used for schematization purposes. The grain size for the non-cohesive class was increased to $d_{50} = 400\,\mu m$ after an initial calibration study based on the observed morphological changes, as $d_{50} = 300\,\mu m$ had caused excess sedimentation and erosion. This modification did not affect the sediment transport validation of our model carried out for MOW1 station.

Comparison between observed (Fig. 9a) and modelled (Fig. 9b) morphological changes between 1984 and 2022 indicate that the accelerated model predicts higher magnitudes of morphological evolution relative to the measurements. A comparison of the deposition/erosion patterns reveals that the model can reproduce erosion-deposition locations with $A_{m,\%} = 61.09\%$ accuracy (Fig. SI–11). The mismatch is caused by the model behaving more depositionally compared to the observations ($A_{fd,\%} = 29.36\%$ and $A_{fe,\%} = 9.53\%$). Although the model accurately reproduces large-scale north-easterly movement as reported by Dujardin et al. (2023), it predicts deposition on the offshore flanks of the Nieuwpoortbank and the Stroombank, whereas measurements point towards erosion in these areas. Additionally, a comparison in bank migration direction between the model and

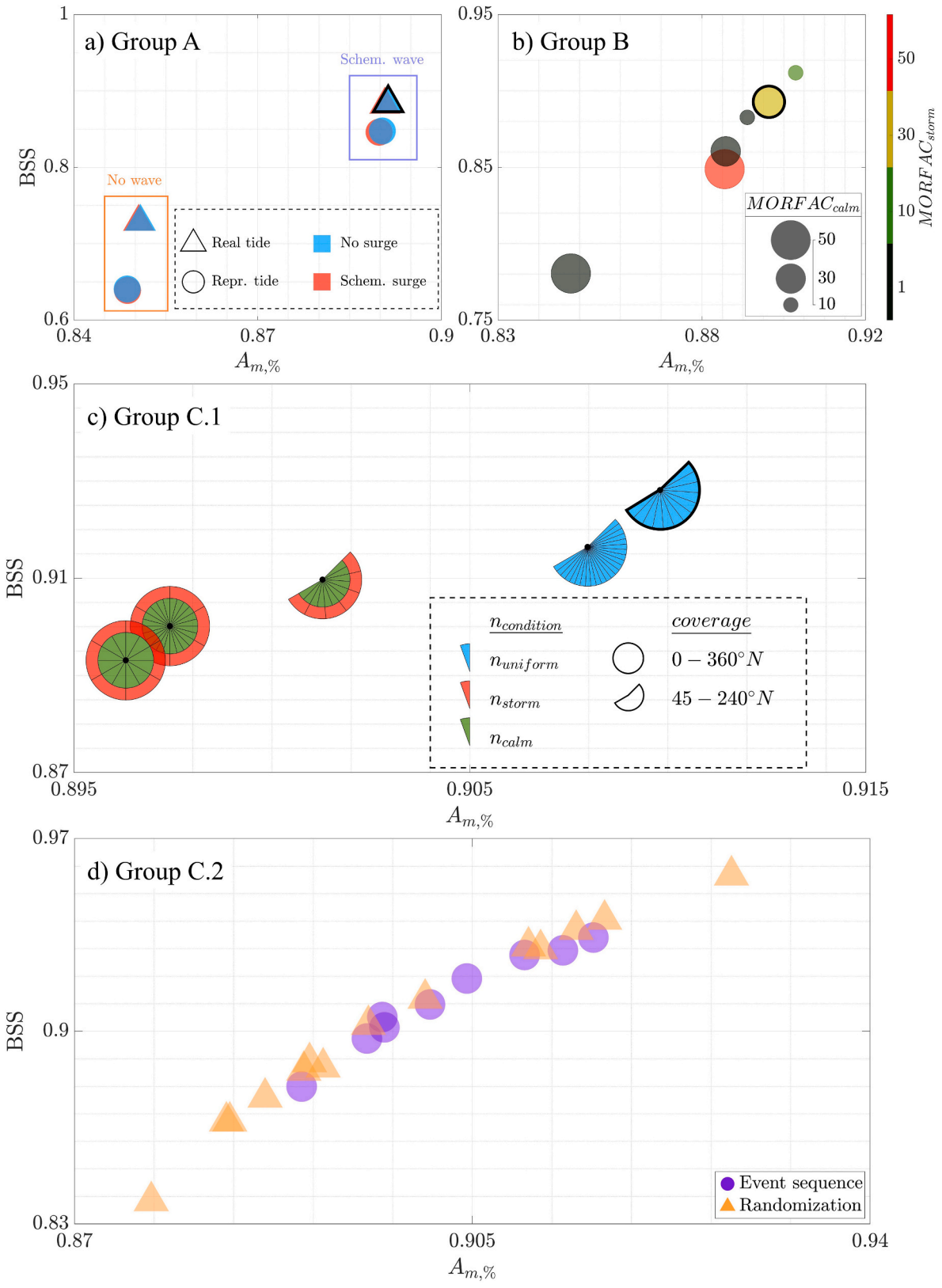

Fig. 7. Summary of the *MORFAC* optimization study. The best run carried on to the next tests is highlighted with the thick black outline. (a) Forcing test performance investigating the impact of the definition of tides (triangle and circle), storm surges (blue and red color), and waves (within the orange or purple rectangle); (b) *MORFAC* value sensitivity investigating the *MORFAC* value during calm (increasing $MORFAC_{calm}$ with increasing bubble size) and storm conditions (the color of the bubbles, i.e., black, green, yellow, and red with increasing $MORFAC_{storm}$); (c) Wave schematization impact on the performance investigating the number of schematized wave conditions (number of pies) with the number of storm (red pies), calm (green pies) or no distinction (blue pies) and directional wave coverage (full or partial circle) that are used for the synthetic wave time series generation; (d) Event sequence test (purple circles) investigating the change of sequence of the wave events selected with the same seed, and randomization of the event selection test (orange triangles) that selects random events based on different random seeds.

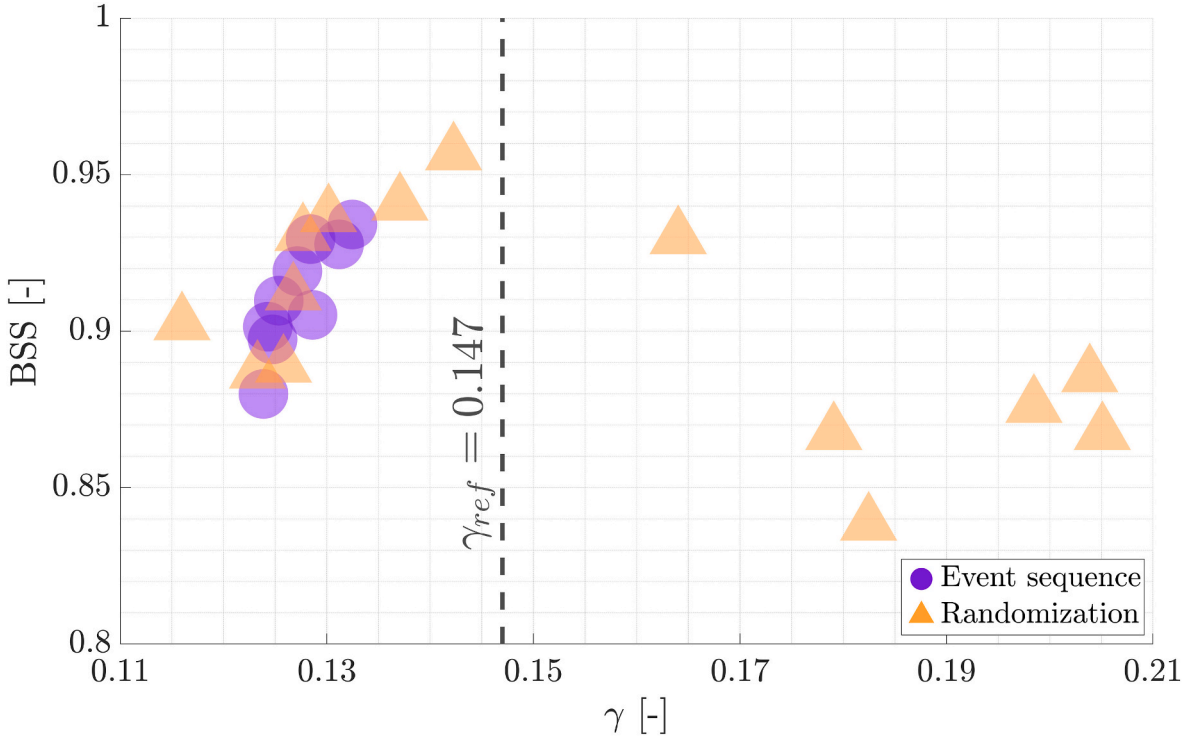

Fig. 8. Sensitivity of the *BSS* value to the γ coefficient at the boundary (higher value indicates that higher waves occur simultaneously with higher tidal ranges).

the observations reveals a clear mismatch. The model is able to capture the southeasterly migration of Nieuwpoortbank as seen in observations, though it fails to predict the onshore migration of the Stroombank (Fig. 9a and b, magenta and light blue arrows, respectively, and Fig. 10a). The discrepancy in the behaviour of the Stroombank is further discussed in Section 4.2.

4. Discussion

4.1. MORFAC optimization

Across Groups A-C, the sensitivity tests collectively show that in the present system, predictive skill is based on three coupled choices: (i) how well the hydrodynamic model resolves spring-neap variability and wave-tide interactions (γ-factor), (ii) the degree to which the wave time series represents the underlying probability distribution and associated wave statistics and (iii) the *MORFAC* value. The model's increased performance when including waves suggests that morphological change in the region of interest is shaped by a combination of both current (tidal and wave induced) and wave forcing. This is in agreement with the classification by Hayes (1979), which would classify the Belgian Coast as a mixed-energy tide-dominated system. In our case study, we found a direct link between predictive performance and the newly defined γ-factor. A comparison of the γ-factor between the benchmark and accelerated runs highlights the importance of the timing between high-energy wave events and tidal cycles. Modelled wave heights at the Westhinder station (2013-2023) of the benchmark run confirm that morphologically significant wave events predominantly occur when the modelled tidal range exceeds 3.5 m (Fig. SI–12). The γ_{ref} value calculated as 0.147 with the benchmark model boundary conditions at Westhinder using waves larger than 1.4 m (the smallest schematized wave condition to mobilize a sandy bed with $d_{50} = 300\,\mu m$ at 10 m depth computed by using Eq. (A.1-6)), is nearly identical to the best accelerated run ($\gamma = 0.142$). Model performance decreases above or below this range, indicating that preserving the natural alignment of energetic wave and tidal conditions, as observed in the benchmark model, is essential when generating forcing data for morphodynamic upscaling.

We expect that the γ-factor may play an even more significant role in morphodynamic predictions with increasing importance of wave forcing such as within mixed-energy wave-dominated systems. Therefore, we propose that the newly developed γ parameter can become an essential tool for enhancing the accuracy and reliability of morphodynamic predictions across all mixed-energy environments. Our results suggest that hydrodynamic forcing, spring-neap tides and high-low wave energy, introduces morphological path dependency, where morphological evolution depends on the sequence and co-occurrence of hydrodynamic conditions, which is consistent with Schrijvershof et al. (2023). Since water levels influence wave transformation and, in turn, sediment transport, the same wave conditions at the boundary can produce different morphological responses depending on when they occur during the tidal cycle. Although previous studies have investigated the impact of wave-chronology on the morphological evolution (Dissanayake et al., 2015; Southgate, 1995), to the best of our knowledge, the effect of interactions between dominant forcings, i.e., spring-neap tidal cycles in combination with synthetic wave time series, on the morphological predictions have not yet been described. In the event-sequencing tests (C.2), the same set of schematized wave conditions and identical numbers of realizations were used, with the only difference being the order of events. In contrast, the randomization tests, although based on the same parent probability distribution, introduce variability in the number of realizations per wave condition due to stochastic selection. This likely explains the broader spread in model performance observed in these 14 randomization tests.

Results of Group A (Fig. 7a) show that representative tides produce similar flow velocities in each tidal cycle, leading to relatively less time variation in bed shear stresses in each cycle. This approach smooths out the high shear stress values normally experienced during spring tides, resulting in less pronounced morphological patterns. Storm surges have little impact on model performance, which may be due to the absence of intertidal areas within the analysis polygon, where storm surge effects might have been stronger. Within Group B results (Fig. 7b), performance

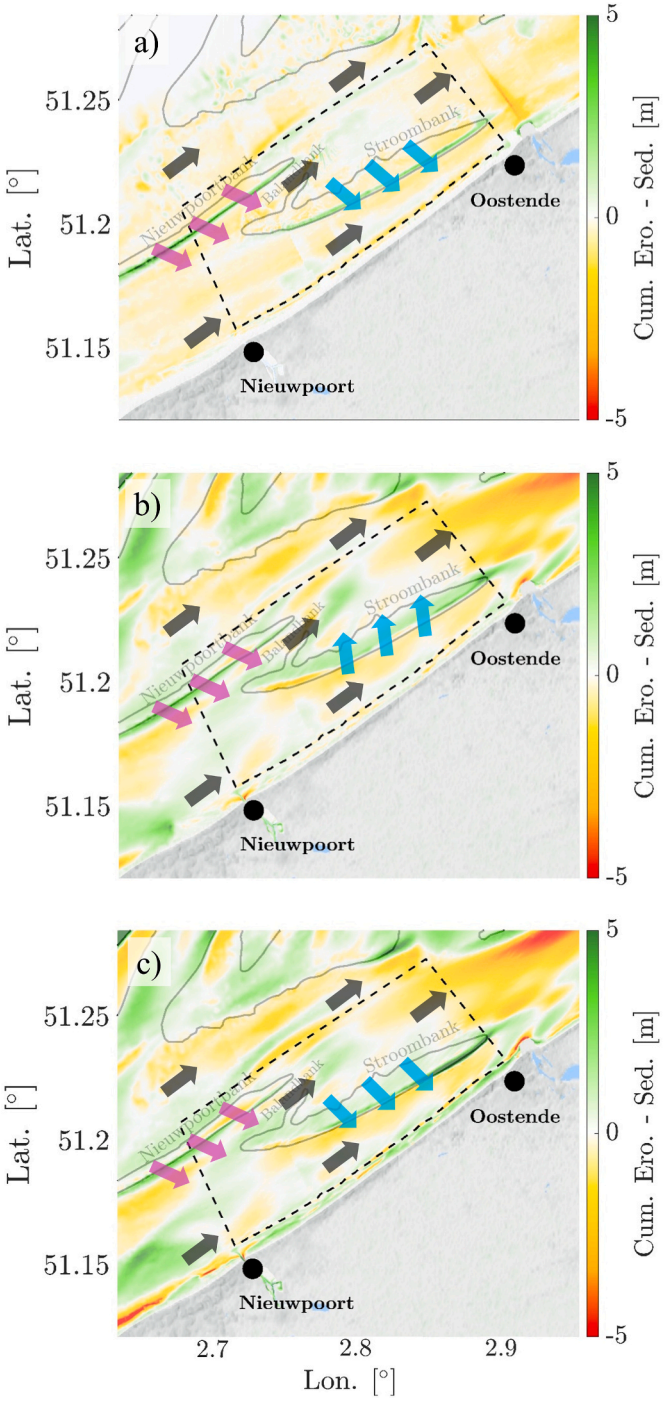

Fig. 9. Cumulative sedimentation and erosion between 1984 and 2022 (a) reconstructed by (Dujardin et al., 2023) and (b) hindcasted without, and (c) with implemented cross-shore sediment transport processes. Arrows show the bedform migration directions of Stroombank (light blue) and Nieuwpoortbank (magenta).

decrease with increasing *MORFAC* value is attributed to two reasons. Firstly, as indicated in previous studies, a high *MORFAC* will introduce larger bed level changes per morphological time step, which potentially changes the flow-field, thus distorting the morphological feedback and reducing the model accuracy (Roelvink, 2006). Secondly, increasing the *MORFAC* value reduces computational time and concurrently shortens the length of the synthetic wave time series applied at the boundary. As the length of the time series decreases, the random sampling from the probability distribution becomes less representative, which might underrepresent the contribution of extreme wave conditions to the morphological evolution. On the other hand, the performance decrease observed with a reduced *MORFAC* value during storm conditions is linked to the fact that the impact of frequently occurring calm wave conditions on the morphology is amplified by the chosen *MORFAC*. More specifically, the occurrence of calm and storm events introduced in the probability distribution is offset by increasing the *MORFAC* value during calm conditions, thus giving storm conditions a relatively lower morphological significance than in the reference dataset. Therefore, we recommend that when wave forcing probability is accounted for in morphological upscaling to adjust the model wave forcing, it should be applied within a framework that uses a constant *MORFAC*. Group C.1 results (Fig. 7c) show that separating storm and calm conditions can produce storm classes with very low occurrence probabilities, sometimes even entirely absent from the synthetic series. A uniform schematization avoids this issue by keeping high-energy events within the main distribution. Likewise, increasing the number of discretized wave classes forces more conditions into a fixed-length series, reducing how well their probabilities are represented. In parallel, including outgoing boundary waves reduces performance, as they do not contribute to sediment transport and instead take up time in the series, reducing the duration of morphologically effective incoming waves. Ultimately, to ensure realistic morphological upscaling, the schematized wave forcing should contain enough morphodynamically significant conditions, i.e., waves entering the domain with probabilities high enough to be adequately represented in the synthetic time series.

In summary, predicting morphological development in mixed-energy systems by incorporating schematized waves in morphological simulations involves a trade-off between the dominant hydrodynamic processes, the number and directionality of wave conditions, the representation of rare high-energy events, and the chosen morphological acceleration factor (*MORFAC*). Overall, non-interacting waves leaving the domain should be excluded, and the representativeness of the synthetic wave time series should depend on the correct representation of both wave statistics and wave-tide interaction. This means that the *MORFAC* value should be selected in conjunction with the dominant forcing factors (tides and waves) and their interactions (γ-factor). We, therefore, recommend determining a reference interaction factor (γ_{ref}) and generating synthetic wave series with comparable γ values, where morphological evolution is governed by nonlinear wave-tide interactions.

4.2. *Model application on predicting the multi-decadal morphological evolution of the Belgian Coast*

Given the limited availability of subsurface data, the presented results in our study represent the most probable morphological trajectory based on the current optimal parameter set. The comparison between the optimized model and field data (Fig. 9a and b and Fig. 10a) demonstrates that the model is partially able to represent the patterns of morphological development over the past 38 years. However, two main shortcomings can be identified: (i) the magnitudes of the predicted sedimentation and erosion are overestimated compared to the observations and (ii) the direction of the movement of the Stroombank is misrepresented in the model predictions (benchmark run and accelerated prediction).

(i) We expect some mismatch between model predictions and observations due to the wide-reaching human activities that are not incorporated in the model such as dredging, dumping and nourishments carried out in the area of interest, which was shown to be able to alter bed level changes by 16% (Dujardin et al., 2023). Although their influence is considered of secondary importance, our model omits the hard structures (e.g. breakwater and groynes) that could influence the sediment transport pathways,

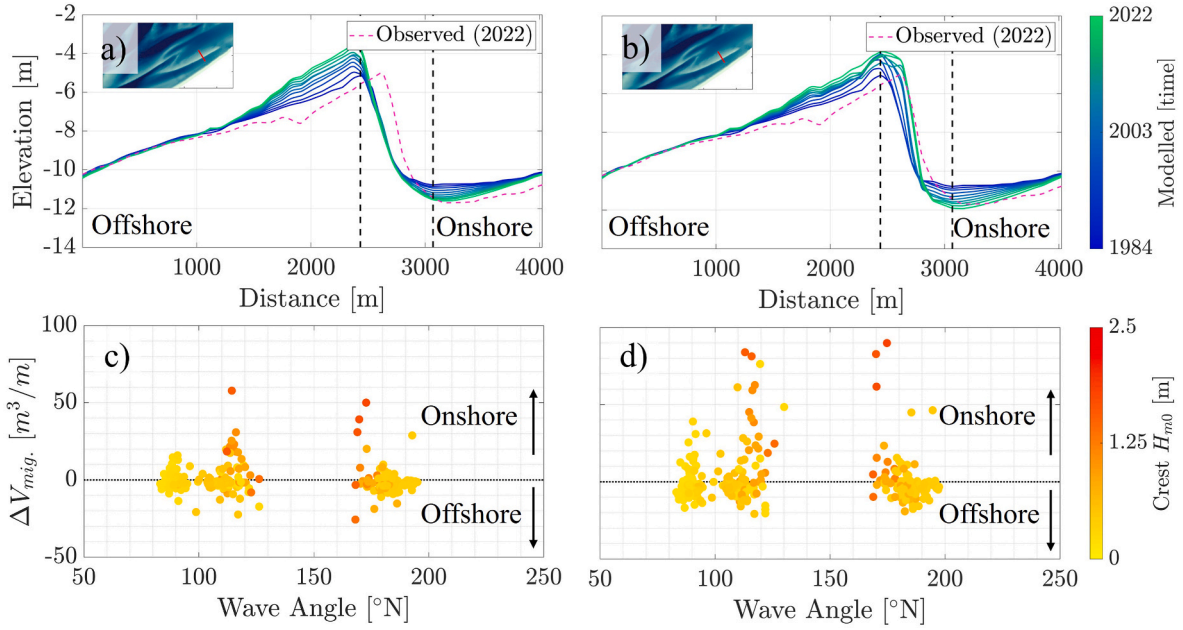

Fig. 10. (a) Stroombank cross-shore profile evolution compared to the reconstructed profile (magenta) (Dujardin et al., 2023) at the end of the simulation without and (b) with cross-shore sediment transport; (c) modelled volumetric migration rate between the two vertical dashed lines shown in the profile evolution plots without and (d) with cross-shore sediment transport processes in relation with modelled significant wave height at the bank crest (from lower to higher with yellow to red colours) and wave direction.

leading to an indirect impact on the morphological evolution within the comparison area. The seabed between Nieuwpoort and Oostende is mainly sandy with small amounts of mud, so sediment erosion in the model is largely driven by sand. Comparing the modelled bed shear stresses (from currents and waves) with the critical shear stress for $d_{50} = 400\ \mu m$ estimated using Soulsby (1997) shows that the sandy bed is almost always mobilized during both spring and neap tides. This causes excessive sediment movement, with material eventually settling in calmer areas, mainly along the offshore flanks of the sandbanks (Fig. 9b). This suggests that either seabed sediment characteristics and/or the choice of equilibrium sediment concentration formulation would need additional refinement, which would in turn improve prediction of the bed level changes. As reported by Kolokythas et al. (2023), the Soulsby-van Rijn formulation, which is still the state-of-the-art equation for wave and current induced sand transport, tends to overestimate morphological changes, particularly in deeper areas. This issue could potentially be mitigated by either adopting an alternative formulation or applying a calibration factor to reduce the equilibrium sediment concentration computed by GAIA, as suggested by Kolokythas et al. (2024a) and Dastgheib (2012). However, such a reduction might also lower the computed SPM concentrations, which could negatively impact the sediment transport validation of the model. It is also important to note the uncertainties in the measurements as pointed out by Dujardin et al. (2024), including errors due to measuring technique, horizontal and vertical reference conversions, digitization of the old maps, data gridding, and daily differences between consecutive surveys, introducing significant uncertainties in the observations.

(ii) The discrepancy between predicted and observed cross-shore migration of the Stroombank highlights an important shortcoming of the modelling framework. The sediment-transport module GAIA transports sediment in the direction of the flow computed by the flow-module TELEMAC2D. As such, cross-shore sediment transport, and thus cross-shore bank migration, can only occur if there is a net cross-shore flow component. Analysis of 30-day averaged tidal ellipses (Fig. SI–13) supports this interpretation. Over the Nieuwpoortbank, the ellipses display a strong cross-shore flow component, and the orientation of their major axes suggests a shoreward and north-easterly flow pattern, which are consistent with the correctly modelled onshore migration of the bank. In contrast, while still being very strong in the longshore direction, the ellipses over the Stroombank show weaker cross-shore flow components compared to the ones over the Nieuwpoortbank, and their major axes tend to have a more offshore-oriented direction on the Stroombank crest. This offshore-dominant cross-shore and northeast dominant longshore flow likely explains why the modelled migration of the Stroombank is in the offshore and north-easterly direction, the former being contrary to field observations. This raises the question of which additional processes govern the onshore migration of the Stroombank that are not represented in the current model configuration.

Investigation of the morphological changes during a storm coming from the north-north west direction showed that the cross-shore movement of the Stroombank towards the coast could be triggered by the wave induced sediment transport. This is why we expect that the mismatch might be partly explained by the underrepresentation of wave direction on the sediment transport direction in the version of sediment transport module, GAIA, used in this study. In this context, the implementation of wave-induced cross-shore sediment transport processes could improve the computed sediment transport directions and might potentially improve the predicted morphological patterns. Therefore, following Fonias et al. (2021), we modified the convection velocity by incorporating wave non-linearity (Ruessink et al., 2012) and Stokes-drift-induced return flow effects (Phillips, 1967). The modified convection velocity direction was also used to adjust the direction of the bedload vector assuming that the bedload vector followed the convection velocity vector direction, while retaining the bedload quantity computed by the sediment-transport module GAIA (see Eq. (B.1-4)). We verified the implementation using the BCM with real boundary conditions, setting the skewness (A_{sk}) and asymmetry (A_{as}) calibration factors

to 1.0, and running the model for the period 2013-2018. This comparison reveals that the improved model was able to reproduce the correct migration direction of the Stroombank (Fig. SI–14 and Fig. SI–15), while maintaining its accuracy for the Nieuwpoortbank.

On a larger spatial scale, the new implementation improved the model performance by reducing the mean bias in the cumulative sedimentation and erosion magnitudes between observations and models within the comparison zone from 0.23 m to 0.20 m. Additionally, the updated model was able to reproduce the cross-shore migration direction and onshore flank position of the investigated profile accurately (Fig. 10b). On the other hand, the modelled depth of the bank crest for the investigated profile reaches as low as −4 m MSL, which is shallower than the −5 m MSL observed depth. In reality, wave breaking takes place on the Stroombank during storms and low tide conditions (Peelman, 2022) which could limit the vertical growth of the bank. A similar physical effect could be reproduced in the model by incorporating a more detailed representation of breaking-related processes, such as breaking induced turbulence and surface rollers, as implemented for GAIA in a separate study (Kolokythas et al., 2024b). Our analyses demonstrates that waves are a key control on the cross-shore migration of the Stroombank, whereas tides predominantly explain its longshore migration. In contrast, at the Nieuwpoortbank, the cross-shore and longshore migrations are primarily tide-driven, with wave effects acting as a secondary influence.

4.2.1. *Equifinality phenomena of long-term morphological models*

An investigation of the modelled wave direction, wave height, and volumetric migration of the Stroombank (i.e. the volumetric change between the initial crest and trough of the bank (Fig. SI–14b)), previously suggested that the cross-shore bank movement was governed by relatively energetic wave events attacking from a mean angle between 110 and 200° N. However, it is noticed that these wave directions, i.e., 110-200° N, are poorly represented in the schematized wave conditions (Fig. 10c and d) used throughout the optimization, as they tend to fall near the edges of the directional bins (Fig. 5a). Despite this, applying the cross-shore implementation ($A_{sk} = A_{as} = 1.0$) with the schematized wave conditions to the validation run (1984-2022) still yielded in correct migration directions. This raised a critical question: would a wave schematization confined strictly to the 110-200° N range still induce correct migration through forcing alone?

To investigate this further, we conducted a final sensitivity analysis with two more model runs using a new wave schematization covering only the 110-200° N range (i) without, and (ii) with cross-shore sediment transport processes. The new wave time-series using these confined directions produced a less realistic wave-tide timing with reduced $\gamma_{110-200°N} = 0.124$, which moved further away from $\gamma_{ref} = 0.143$ compared to the original $\gamma_{45-240°N} = 0.139$. The profile results (Fig. SI-16e & g) revealed that while correct migration could be reproduced even more accurately by confining the schematization to the 110-200° N range, including cross-shore sediment transport processes in this specific case actually reduced model reliability. This sensitivity analysis highlights an important case of model equifinality, where bank migration was driven either through the inclusion of cross-shore sediment transport with a more realistic hydrodynamic conditions or the selective filtering of wave schematization. While the latter reproduced the observed morphological migration without additional parameterization, it introduced a significant forcing bias. This not only degrades the representation of the observed waves but also negatively impacts the wave-tide timing by shifting γ-factor further away from γ_{ref}. Ultimately, this sensitivity analysis suggests that wave-tide timing (γ-factor) must take precedence over morphological fit. Prioritizing the correct representation of hydrodynamical forcing and their interactions can prevent the model from achieving the “right result for the wrong reason,” ensuring greater reliability for long-term morphodynamic predictions.

5. Conclusion

In this study, a hydro-morphodynamic model using the TELEMAC-suite was developed to predict decadal-scale morphodynamic developments of the Belgian Continental Shelf. The model results suggest that the present model can accurately capture the main hydro- and sediment dynamics both during calm and storm conditions. While synthetic storm surge had little impact within the comparison area, the MORFAC optimization procedure indicates that, in mixed-energy systems, morphological predictions should be optimized by accurately representing the wave climate in combination with tidal fluctuations, including spring-neap variations, instead of a single representative tide. For this purpose, our study defined a new parameter, the γ-factor, which allows optimizing the co-occurrence of waves and tides with existing field data to retain morphological path-dependency.

Following the optimization study, the proposed model was applied to simulate the morphological evolution of a section of the Belgian coast between Nieuwpoort and Oostende over the period 1984-2022. The model successfully reproduced the main observed morphological patterns of the Nieuwpoortbank, but failed to capture the observed coastward migration of the Stroombank. Further investigation of the model runs incorporating real boundary conditions revealed that the observed cross-shore migration of the eastern half of the Stroombank can be explained by the wave induced cross-shore sediment transport processes. Implementation of those processes in GAIA enabled to accurately reproduce the shoreward migration of the Stroombank including the positions of the crest and onshore flank of the selected profile and to identify the local processes driving the Nieuwpoortbank (mainly tides) and Stroombank migration (waves in the cross-shore, tides in the longshore direction). On a broader level, the issue of equifinality in long-term morphological modelling strategies was briefly demonstrated and discussed. Ultimately, the optimization strategy for the MORFAC method presented here is applicable beyond TELEMAC/GAIA and are relevant to any long-term coastal modelling effort where wave and tide driven sediment transport plays a significant role.

CRediT authorship contribution statement

Yağız Arda Çiçek: Writing – original draft, Visualization, Validation, Methodology, Investigation, Formal analysis, Conceptualization. **Jaak Monbaliu:** Writing – review & editing, Supervision. **Erik Toorman:** Writing – review & editing, Supervision. **Víctor Cartelle:** Writing – review & editing. **Ruth Plets:** Writing – review & editing. **Nathalie Pil:** Writing – review & editing. **Soetkin Vervust:** Writing – review & editing. **Christian Schwarz:** Writing – review & editing, Supervision, Methodology.

Declaration of competing interest

The authors declare that they have no known competing financial interests or personal relationships that could have appeared to influence the work reported in this paper.

Acknowledgements

This work is funded by the Strategic Basic Research (SBO) programme of the Fund for Scientific Research (FWO) as part of the project 'TESTEREP: The evolution of the Flemish seascape (5000 BP-present) - Testerep reconstructed for policymaking and public engagement' (Ref. S007522N). The resources and services used in this work were provided by the VSC (Flemish Supercomputer Center), funded by the Research Foundation - Flanders (FWO) and the Flemish Government. The authors would like to thank Vera Van Lancker and Michael Fettweis for their willingness to share their datasets.

Appendix A. Supplementary data

Supplementary data to this article can be found online at https://doi.org/10.1016/j.coastaleng.2026.104989.

Data availability

Data will be made available on request.

References

Adriaens, R., Zeelmaekers, E., Fettweis, M., Vanlierde, E., Vanlede, J., Stassen, P., Elsen, J., Środoń, J., Vandenberghe, N., 2018. Quantitative clay mineralogy as provenance indicator for recent muds in the southern North Sea. Mar. Geol. 398, 48–58. https://doi.org/10.1016/j.margeo.2017.12.011.

Barbier, E.B., Hacker, S.D., Kennedy, C., Koch, E.W., Stier, A.C., Silliman, B.R., 2011. The value of estuarine and coastal ecosystem services. Ecol. Monogr. 81 (1), 169–193. https://doi.org/10.1890/10-1510.

Battjes, J.A., Janssen, J.P.F.M., 1979. Energy loss and Set-Up due to breaking of random waves. In: Proceedings of the Coastal Engineering Conference, Proceedings, pp. 569–587. https://doi.org/10.9753/icce.v16.32.

Bi, Q., Toorman, E.A., 2015. Mixed-sediment transport modelling in Scheldt estuary with a physics-based bottom friction law. Ocean Dyn. https://doi.org/10.1007/s10236-015-0816-z.

Boechat Albernaz, M., Brückner, M.Z.M., van Maanen, B., van der Spek, A.J.F., Kleinhans, M.G., 2023. Vegetation reconfigures barrier coasts and affects tidal basin infilling under sea level rise. J. Geophys. Res. Earth Surf. 128. https://doi.org/10.1029/2022JF006703.

Breugem, W.A., Fonias, E., Wang, L., Bolle, A., Kolokythas, G., De Maerschalck, B., 2019. TEL2TOM: coupling TELEMAC2D and TOMAWAC on arbitrary meshes. XXVth TELEMAC-MASCARET User Conf. Toulouse 15–17.

Dastgheib, A., 2012. Long-Term Process-based Morphological Modeling of Large Tidal Basins. IHE Delft Institute for Water Education.

Dastgheib, A., Roelvink, J.A., Wang, Z.B., 2008. Long-term process-based morphological modeling of the Marsdiep Tidal Basin. Mar. Geol. 256, 90–100. https://doi.org/10.1016/j.margeo.2008.10.003.

De Maeyer, P., Wartel, S., 1988. Relation between superficial grainsize and morphological features of the coastal ridges off the Belgian coast. Tide-Influenced sediment. Environ. Facies 101–112.

De Vriend, H.J., Capobianco, M., Chesher, T., De Swart, H.E., Latteux, B., Stive, M.J.F., 1993a. Approaches to long-term modelling of coastal morphology: a review. Coast. Eng. 21, 225–269. https://doi.org/10.1016/0378-3839(93)90051-9.

De Vriend, H.J., Zyserman, J., Nicholson, J., Roelvink, J.A., Péchon, P., Southgate, H.N., 1993b. Medium-term 2DH coastal area modelling. Coast. Eng. 21, 193–224. https://doi.org/10.1016/0378-3839(93)90050-I.

Deleu, S., Van Lancker, V., Van Den Eynde, D., Moerkerke, G., 2004. Morphodynamic evolution of the kink of an offshore tidal sandbank: the Westhinder bank (Southern North Sea). Cont. Shelf Res. 24, 1587–1610. https://doi.org/10.1016/j.csr.2004.07.001.

Dissanayake, P., Brown, J., Karunarathna, H., 2015. Impacts of storm chronology on the morphological changes of the Formby beach and dune system , UK 1533–1543. https://doi.org/10.5194/nhess-15-1533-2015.

Dujardin, A., Houthuys, R., Nnafie, A., Röbke, B., van der Werf, J., de Swart, H.E., Biernaux, V., De Maerschalck, B., Dan, S., Verwaest, T., 2024. MOZES – Research on the Morphological Interaction Between the Sea Bottom and the Belgian Coastline: Working Year 2. Version 0.1. FHR Reports, 20_079_2. Antwerp.

Dujardin, A., Houthuys, R., Nnafie, A., Röbke, B., van der Werf, J., de Swart, H.E., Biernaux, V., De Maerschalck, B., Dan, S., Verwaest, T., 2023. MOZES – Research on the morphological interaction between the sea bottom and the Belgian coastline: working year 1. Version 4.0FH Reports, 20_079_1. Flanders Hydraulics, Antwerp, pp. 114–134.

Eck, V., 1999. De Scheldeatlas, Een Beeld Van Een Estuarium.

Egbert, G.D., Erofeeva, S.Y., 2002. Efficient inverse modeling of barotropic ocean tides. J. Atmos. Ocean. Technol. 19, 183–204. https://doi.org/10.1175/1520-0426(2002)019<0183:EIMOBO>2.0.CO, 2.

Escobar, S., Bi, Q., Fettweis, M., Wongsoredjo, S., Monbaliu, J., Toorman, E., 2023. A dynamic 2DH flocculation model for coastal domains. Ocean Dyn. 73, 333–358. https://doi.org/10.1007/s10236-023-01554-y.

Fettweis, M., Baeye, M., Cardoso, C., Dujardin, A., Lauwaert, B., Van den Eynde, D., Van Hoestenberghe, T., Vanlede, J., Van Poucke, L., Velez, C., Martens, C., 2016. The impact of disposal of fine-grained sediments from maintenance dredging works on SPM concentration and fluid mud in and outside the harbor of Zeebrugge. Ocean Dyn. 66, 1497–1516. https://doi.org/10.1007/s10236-016-0996-1.

Fettweis, M., Nechad, B., Van den Eynde, D., 2007. An estimate of the suspended particulate matter (SPM) transport in the southern North Sea using SeaWiFS images, in situ measurements and numerical model results. Cont. Shelf Res. 27, 1568–1583. https://doi.org/10.1016/j.csr.2007.01.017.

Fonias, E., Breugem, W.A., Wang, L., Wang, L., Bolle, A., Kolokythas, G., De Maerschalck, B., 2021. Implementation of cross-shore processes in GAIA. Proc. Pap. Submitt. to 2020 TELEMAC-MASCARET user Conf. - Oct. 138–143, 2021.

GEBCO Compilation Group, 2020. GEBCO 2020 Grid. https://doi.org/10.5285/a29c5465-b138-234d-e053-6c86abc040b9.

Geuzaine, C., Remacle, J., 2009. Gmsh: a 3-D finite element mesh generator with built-in pre- and post-processing facilities. Int. J. Numer. Methods Eng. 79, 1309–1331. https://doi.org/10.1002/nme.2579.

Guillaume Olivier, M., Leroux, E., Rabineau, M., Le Hir, P., Granjeon, D., Chataigner, T., Beudin, A., Muller, H., 2021. Numerical modelling of a Macrotidal Bay over the last 9,000 years: an interdisciplinary methodology to understand the influence of sea-level variations on tidal currents in the Bay of Brest. Cont. Shelf Res. 231. https://doi.org/10.1016/j.csr.2021.104595.

Hademenos, V., Stafleu, J., Missiaen, T., Kint, L., Van Lancker, V.R.M., 2019. 3D subsurface characterisation of the Belgian Continental Shelf: a new voxel modelling approach. Geol. en Mijnbouw/Netherlands J. Geosci 98. https://doi.org/10.1017/njg.2018.18.

Haerens, P., Bolle, A., Trouw, K., Houthuys, R., 2012. Definition of storm thresholds for significant morphological change of the sandy beaches along the Belgian coastline. Geomorphology 143–144, 104–117. https://doi.org/10.1016/j.geomorph.2011.09.015.

Hayes, M.O., 1979. Barrier island morphology as a function of tidal and wave regime. In: Leatherman, S.P. (Ed.), Barrier Islands from the Gulf of Mexico to the Gulf of St. Lawrence. Academic Press, New York, pp. 1–28.

He, Z., Liang, M., Jia, L., Dong, H., Chen, K., Liu, J., Lin, Y., Ou, J., 2022. Long-term morphological modeling and implication for estuarine regulation of the Modaomen Estuary, Pearl River Delta, China. Appl. Ocean Res. 123. https://doi.org/10.1016/j.apor.2022.103184.

Hersbach, H., Bell, B., Berrisford, P., Hirahara, S., Horányi, A., Muñoz-Sabater, J., Nicolas, J., Peubey, C., Radu, R., Schepers, D., Simmons, A., Soci, C., Abdalla, S., Abellan, X., Balsamo, G., Bechtold, P., Biavati, G., Bidlot, J., Bonavita, M., De Chiara, G., Dahlgren, P., Dee, D., Diamantakis, M., Dragani, R., Flemming, J., Forbes, R., Fuentes, M., Geer, A., Haimberger, L., Healy, S., Hogan, R.J., Hólm, E., Janisková, M., Keeley, S., Laloyaux, P., Lopez, P., Lupu, C., Radnoti, G., de Rosnay, P., Rozum, I., Vamborg, F., Villaume, S., Thépaut, J.N., 2020. The ERA5 global reanalysis. Q. J. R. Meteorol. Soc. 146, 1999–2049. https://doi.org/10.1002/qj.3803.

Hirano, M., 1971. River-bed degradation with armoring. Proc. Japan Soc. Civ. Eng. 1971, 55–65. https://doi.org/10.2208/jscej1969.1971.195_55.

Hoagland, S.W.H., Jeffries, C.R., Irish, J.L., Weiss, R., Mandli, K., Vitousek, S., Johnson, C.M., Cialone, M.A., 2023. Advances in morphodynamic modeling of coastal barriers: a review. J. Waterw. Port, Coast. Ocean Eng. 149, 1–27. https://doi.org/10.1061/jwped5.wweng-1825.

Hu, P., Ji, A., Li, W., Tang, X., Xiao, W., Cao, Z., 2025. Capacity and Noncapacity Sediment Transport Characteristics in the Overtopping-Induced Dam-Breaching Process, 151, pp. 1–12. https://doi.org/10.1061/JHEND8.HYENG-13985.

Kolokythas, G., Breugem, A., De Maerschalck, B., 2024a. Morphodynamic modelling of the Belgian Coastal zone: sub report 4 – Cross-shore transport modelling with GAIA: Ostend model. Version 4.0. FH Reports, 21_104_4. Antwerp 47–49.

Kolokythas, G., Breugem, A., De Maerschalck, B., 2024b. Morphodynamic Modelling of the Belgian Coastal Zone: Sub Report 3 – Implementation and Testing Cross-shore Transport Processes in GAIA, pp. 15–16. Antwerp, Belgium.

Kolokythas, G., De Maerschalck, B., Wang, L., Fonias, S., Breugem, A., Vanlede, J., Mostaert, F., 2021. Modelling Belgian Coastal zone and Scheldt mouth area: sub report 12: Scaldis-Coast model – model setup and validation of the 2D hydrodynamic model. FHR Reports, 15_068_12. Flanders Hydraul. Res. Antwerp Reprod 1–65. Version 4.0.

Kolokythas, G., Fonias, S., Wang, L., De Maerschalck, B., Vanlede, J., 2023. Modelling Belgian Coastal zone and Scheldt mouth area: sub report 14: Scaldis-Coast model – model setup and validation of the morphodynamic model. FH Reports, 15_068_14. Flanders Hydraul. Antwerp 1–214. Version 4.0.

Kroon, A., Christiaanse, J.C., Luijendijk, A.P., Schipper, M.A.d., Ranasinghe, R., 2025. Parameter uncertainty in medium-term coastal morphodynamic modeling. Sci. Rep. 15, 1–15. https://doi.org/10.1038/s41598-025-02300-8.

Lanckneus, J., Van Lancker, V., Moerkerke, G., Van den Eynde, D., Fettweis, M., De Batist, M., Jacobs, P., 2001. Investigation of the Natural Sand Transport on the Belgian Continental Shelf: BUDGET (Beneficial Usage of Data and geo-environmental Techniques). Brussel.

Latteux, B., 1995. Techniques for long-term morphological simulation under tidal action. Mar. Geol. 126, 129–141. https://doi.org/10.1016/0025-3227(95)00069-B.

Le Hir, P., Cayocca, F., Waeles, B., 2011. Dynamics of sand and mud mixtures: a multiprocess-based modelling strategy. Cont. Shelf Res. 31, 135–149. https://doi.org/10.1016/j.csr.2010.12.009.

Lesser, G.R., Roelvink, J.A., van Kester, J.A.T.M., Stelling, G.S., 2004. Development and validation of a three-dimensional morphological model. Coast. Eng. 51, 883–915. https://doi.org/10.1016/j.coastaleng.2004.07.014.

Lyu, B., Li, J., Hu, P., Cao, Z., Liu, H., 2024. High-resolution hydro-sediment-morphodynamic modelling of a meandering river reach with mid-channel bars on multiyear timescales : a case study of Shashi Reach in Middle Yangtze River 635. https://doi.org/10.1016/j.jhydrol.2024.131167.

Matheen, N., Harley, M.D., Turner, I.L., Splinter, K.D., Simmons, J.A., Thran, M.C., 2021. Bathymetric data requirements for operational coastal erosion forecasting using xbeach. J. Mar. Sci. Eng. 9. https://doi.org/10.3390/jmse9101053.

Mathew, R., Winterwerp, J.C., 2022. Morphodynamic modeling and morphological upscaling in a fine sediment system. Adv. Water Resour. 166, 104224. https://doi.org/10.1016/j.advwatres.2022.104224.

Montreuil, A.-L., Delgado, R., Van Oyen, T., Dan, S., Vereecken, H., Deschamps, M., Verwaest, T., Mostaert, F., 2015. Sinterklaas Storm Effects on Hydrodynamics and Morphology. Antwerp, Belgium.

Neumann, B., Vafeidis, A.T., Zimmermann, J., Nicholls, R.J., 2015. Future coastal population growth and exposure to sea-level rise and coastal flooding - a global assessment. PLoS One 10. https://doi.org/10.1371/journal.pone.0118571.
Partheniades, E., 1965. Erosion and deposition of cohesive soils. J. Hydraul. Div. 91, 105–139. https://doi.org/10.1061/JYCEAJ.0001165.
Pawlowicz, R., Beardsley, B., Lentz, S., 2002. Classical tidal harmonic analysis including error estimates in MATLAB using T_TIDE. Comput. Geosci. 28, 929–937. https://doi.org/10.1016/S0098-3004(02)00013-4.
Peelman, M., 2022. Analyse Van Veldmetingen Van Korte Zeegolven Gaande Van Offshore Tot Aan Living Lab Raversijde.
Pezerat, M., Bertin, X., Martins, K., Mengual, B., Hamm, L., 2021. Simulating storm waves in the nearshore area using spectral model: current issues and a pragmatic solution. Ocean Model. 158, 101737. https://doi.org/10.1016/j.ocemod.2020.101737.
Phillips, O.M., 1967. The dynamics of the upper ocean. Journal of Fluid Mechanics. Cambridge University Press. https://doi.org/10.1017/S0022112067211193.
Pineau-Guillou, L., Delouis, J.M., Chapron, B., 2023. Characteristics of storm surge events along the North-East Atlantic coasts. J. Geophys. Res., Oceans 128, 1–16. https://doi.org/10.1029/2022JC019493.
Ranasinghe, R., Swinkels, C., Luijendijk, A., Roelvink, D., Bosboom, J., Stive, M., Walstra, D., 2011. Morphodynamic upscaling with the MORFAC approach: dependencies and sensitivities. Coast. Eng. 58, 806–811. https://doi.org/10.1016/j.coastaleng.2011.03.010.
Roelvink, D., Huisman, B., Elghandour, A., 2018. Efficient modelling of complex coastal evolution at monthly to century time scales. Sixth Int. Conf. Estuaries Coasts 1–10.
Roelvink, D., Reniers, A., van Dongeren, A., van Thiel de Vries, J., McCall, R., Lescinski, J., 2009. Modelling storm impacts on beaches, dunes and barrier islands. Coast. Eng. 56, 1133–1152. https://doi.org/10.1016/j.coastaleng.2009.08.006.
Roelvink, J.A., 2006. Coastal morphodynamic evolution techniques. Coast. Eng. 53, 277–287. https://doi.org/10.1016/j.coastaleng.2005.10.015.
Roelvink, J.A., Jeuken, M.C.J.L., Van Holland, G., Aarninkhof, S.G.J., Stam, J.M.T., 2001. Long-term, process-based modelling of complex areas. In: Coastal Dynamics 2001. American Society of Civil Engineers (ASCE), pp. 383–392. https://doi.org/10.1061/40566(260)39.
Ruessink, B.G., Ramaekers, G., Van Rijn, L.C., 2012. On the parameterization of the free-stream non-linear wave orbital motion in nearshore morphodynamic models. Coast. Eng. 65, 56–63. https://doi.org/10.1016/j.coastaleng.2012.03.006.
Schrijvershof, R.A., van Maren, D.S., Torfs, P.J.J.F., Hoitink, A.J.F., 2023. A synthetic spring-neap tidal cycle for long-term morphodynamic models. J. Geophys. Res. Earth Surf. 128. https://doi.org/10.1029/2022JF006799.
Shaeri, S., Etemad-Shahidi, A., Strauss, D., Tomlinson, R., 2019. Accelerated numerical simulation to investigate morphology changes around small tidal inlets. Coast. Eng. J. 61, 535–558. https://doi.org/10.1080/21664250.2019.1651562.
Shen, X., Lee, B.J., Fettweis, M., Toorman, E.A., 2018. A tri-modal flocculation model coupled with TELEMAC for estuarine muds both in the laboratory and in the field. Water Res. 145, 473–486. https://doi.org/10.1016/j.watres.2018.08.062.
SHOM, 2021. Carte Sédimentaire Mondiale - Prépaquet.
Smagorinsky, J., 1963. General circulation experiments with the primitive equations. Mon. Weather Rev. 91, 731–732. https://doi.org/10.1126/science.12.306.731-a.
Soulsby, R., 1997. Dynamics of Marine Sands: A Manual for Practical Applications, pp. 182–184.
Southgate, H.N., 1995. The effects of wave chronology on medium and long term coastal morphology. Coast. Eng. 26, 251–270. https://doi.org/10.1016/0378-3839(95)00028-3.
Steijn, R.C., 1992. Input Filtering Techniques for Complex Morphological Models.
Steijn, R.C., 1989. Schematization of the Natural Conditions in multi-dimensional Numerical Models of Coastal Morphology.
Sutherland, J., Peet, A.H., Soulsby, R.L., 2004. Evaluating the performance of morphological models. Coast. Eng. 51, 917–939. https://doi.org/10.1016/j.coastaleng.2004.07.015.
Tassi, P., Benson, T., Delinares, M., Fontaine, J., Huybrechts, N., Kopmann, R., Pavan, S., Pham, C.T., Taccone, F., Walther, R., 2023. GAIA - a unified framework for sediment transport and bed evolution in rivers, coastal seas and transitional waters in the TELEMAC-MASCARET modelling system. Environ. Model. Software 159, 105544. https://doi.org/10.1016/j.envsoft.2022.105544.
Toorman, E.A., 2000. Modelling of turbulence damping in sediment-laden flow. Part 2 Suspen. Capacity Uniform Shear Flows 23.
Van Lancker, V., 1999. Sediment and morphodynamics of a siliciclastic near coastal area, in relation to hydrodynamical and meteorological conditions: belgian Continental shelf. PhD thesis. Universiteit Gent, p. 104.
Van Lancker, V., Du Four, I., Verfaillie, E., Deleu, S., Schelfaut, K., Fettweis, M., Van den Eynde, D., Francken, F., Monbaliu, J., Giardino, A., Portilla, J., Lanckneus, J., Moerkerke, G., Degraer, S., 2007. Management, Research and Budgetting of Aggregates in Shelf Seas Related to end-users (Marebasse) 139.
Van Maren, D.S., Vroom, J., Fettweis, M., Vanlede, J., 2020. Formation of the Zeebrugge coastal turbidity maximum: the role of uncertainty in near-bed exchange processes. Mar. Geol. 425. https://doi.org/10.1016/j.margeo.2020.106186.
Vuik, V., Kuijper, B., Geerse, C.P.M., Strijker, B., Gautier, C., Trouw, K., Vanneste, D., Suzuki, T., Nossent, J., Thoon, D., De Roo, S., Mostaert, F., 2020. Het Hydraulisch Randvoorwaardenboek (2020): rapport 18_037_4.
Wang, L., Kolokythas, G., Fonias, S., De Maerschalck, B., Vanlede, J., Mostaert, F., 2021. Modelling Belgian Coastal zone and Scheldt mouth area: sub report 13: Scaldis-Coast model – model setup and validation of the wave propagation model. FHR Reports, 15_068_13. Flanders Hydraul. Res. Antwerp 9. Version 4.0.
Wang, L., Zimmermann, N., Trouw, K., De Maerschalck, B., Vanlede, J., 2014. Numerical modelling of long-term morphology in the surf zone of the Belgian coast. In: Lynett, P. (Ed.), Proceedings of the Coastal Engineering Conference. American Society of Civil Engineers (ASCE).
Winter, C., 2007. On the evaluation of sediment transport models in tidal environments. Sediment. Geol. 202, 562–571. https://doi.org/10.1016/j.sedgeo.2007.03.019.
Wright, L.D., Thom, B.G., 2023. Coastal morphodynamics and climate change: a review of recent advances. J. Mar. Sci. Eng. 11. https://doi.org/10.3390/jmse11101997.
Yin, Y., Karunarathna, H., Reeve, D.E., 2019. Numerical modelling of hydrodynamic and morphodynamic response of a meso-tidal estuary inlet to the impacts of global climate variabilities. Mar. Geol. 407, 229–247. https://doi.org/10.1016/j.margeo.2018.11.005.
Zhang, W., Harff, J., Schneider, R., Wu, C., 2010. Development of a modelling methodology for simulation of long-term morphological evolution of the southern Baltic coast. Ocean Dyn. 60, 1085–1114. https://doi.org/10.1007/s10236-010-0311-5.
Zhang, W., Schneider, R., Harff, J., 2012. A multi-scale hybrid long-term morphodynamic model for wave-dominated coasts. Geomorphology 149–150, 49–61. https://doi.org/10.1016/j.geomorph.2012.01.019.
Zhao, Y., Han, Z., Zhang, C., Wang, Y., Zhong, J., Gao, M., 2024. Coastal cultural ecosystem services: a bridge between the natural ecosystem and social ecosystem for sustainable development. Land 13, 1352. https://doi.org/10.3390/land13091352.
Zhao, Z., Hu, P., Li, W., Cao, Z., Li, Y., 2025. Advances in engineering software an engineering-oriented Shallow-water hydro-sediment-morphodynamic model using the GPU-acceleration and the hybrid LTS/GMaTS method. Adv. Eng. Software 200, 103821. https://doi.org/10.1016/j.advengsoft.2024.103821.
Zimmermann, N., Trouw, K., Wang, L., Mathys, M., Delgado, R., Verwaest, T., 2012. Longshore transport and sedimentation in a navigation channel at blankenberge (Belgium). Coast. Eng. Proc. 111. https://doi.org/10.9753/icce.v33.sediment.111.